공학박사 학위논문

Investigation of Animal Models and Surgical Techniques for Development of Retinal Prosthesis

인공시각장치 개발을 위한 동물모델 평가와 수술기법 연구

2019년 2월

서울대학교 대학원

협동과정 바이오엔지니어링 전공
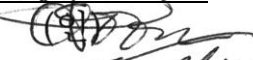
배 소 현

Investigation of Animal Models and Surgical Techniques for Development of Retinal Prosthesis

인공시각장치 개발을 위한 동물모델 평가와 수술기법 연구

지도교수 서 종 모

이 논문을 공학박사 학위논문으로 제출함

2019년 1월

서울대학교 대학원

협동과정 바이오엔지니어링 전공

배 소 현

배소현의 공학박사 학위논문을 인준함

2018년 12월

위 원 장	조 동 일	
부위원장	서 종 모	
위 원	이 종 호	
위 원	전 상 범	
위 원	이 상 민	

Ph.D. DISSERTATION

Investigation of Animal Models and Surgical Techniques for Development of Retinal Prosthesis

February 2019

Interdisciplinary Program in Bioengineering

The Graduate School

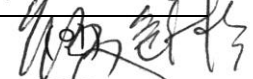Seoul National University

So Hyun Bae

Abstract

Investigation of Animal Models and Surgical Techniques for Development of Retinal Prosthesis

So Hyun Bae

Interdisciplinary Program in Bioengineering

The Graduate School

Seoul National University

Our group has developed and manufactured a seamless liquid crystal polymer (LCP)-based monolithic retinal prosthesis. This device is thin and light which is superior to other prosthetic devices made of ceramic or metal. However, the establishment of reliable and reproducible surgical procedures ensuring the long-term safety of the prosthesis remains a challenge. In the first section of this dissertation, the reproducible surgical techniques were developed to optimize the long-term safety of implantation surgery of our LCP-based retinal prosthesis by *in vivo* experiments. In the pilot study, 2 eyes of 2 New Zealand white rabbits were

operated to implant the prototype LCP-based prosthetic device. The electrode array was inserted into the suprachoroidal space and the system package was anchored on the skull. The interconnection cable was passed through the tunnel under the temporalis muscle. The implantation surgery was successfully performed without any complications. No postoperative complications were detected including intraocular hemorrhage, retinal detachment, wound dehiscence and displacement of the device under fundus examination, optical coherence tomography (OCT) images and x-ray. Next, our group has modified the device to implant the device in the eyeball as a whole. Eleven rabbits were operated for the implantation of totally implantable prosthetic device. The electrode array was inserted into the suprachoroid space and the package was fixed onto the sclera under the conjunctiva. The transition part between the electrode array and package were anchored onto the sclera. The surgical procedures for implantation of the entire system were easily performed in nine eyes (81.8%) without any intraoperative complications. In the other two eyes (18.2%), surgical complications related to electrode insertion, including optic nerve damage and retinal tear, arose. In 10 eyes (90.9%), the devices were well tolerated for at least 3 months. However, in most eyes (nine; 81.8%), two complications began to appear after 3 months, postoperatively, including conjunctival erosion or dehiscence over the package or transition part. The electrode arrays were maintained safely in the suprachoroidal space after surgery without any complications, regardless of the status of the extraocular components in all cases except two intraoperative complications. Although issues related to surgical technique or device configuration were identified, further

technical solution would improve the long-term safety of device implantation. Finally, these experiments would provide a stepping stone to achieve the safe and reproducible surgical techniques for human in the future.

Despite many studies in human and animal models, the pathophysiology of retinal degenerative diseases is not still clear. *In vivo* evaluation of the structural changes of retina is important for understanding the development and progression in retinal degenerative diseases. Currently, OCT is the most useful tool for *in vivo* evaluation of the retinal architecture. However, information is still lacking on the anatomic correspondences with abnormal OCT features in eyes with retinal degenerative diseases. In the second section of this dissertation, the anatomic correlates with pathologic OCT features were investigated supported by electroretinography (ERG) findings in experimental retinal degeneration model induced by intravitreal sodium iodate ($NaIO_3$) administration. Twenty rabbits were underwent unilateral intravitreal injections of four different $NaIO_3$ doses: 0.1, 0.2, 0.4 or 0.8mg (n=5 for each dose). Comprehensive ophthalmic examinations were performed including fundus examination, OCT, ERG and histologic analyses from baseline to 28 days after $NaIO_3$ administration. In the 0.2-mg group, there were transient changes of outer retinal layers on OCT, including an indistinguishable external limiting membrane (ELM) and slightly obscure ellipsoid zone (EZ) without significant changes in the histologic sections. In addition, there was transient reduction of a- and b-wave amplitudes followed by complete restoration at day 28. In the 0.4-mg group, the EZ and ELM became completely indistinguishable as early as day 1,

whereas the histologic analysis showed only slightly disorganized photoreceptor inner and outer segments (IS and OS) with relatively preserved overall laminations of photoreceptor cell nuclei, IS and OS. Damage to outer retinal layers progressed in both the OCT and histologic analyses, leading to complete loss of photoreceptors by day 28. Extreme reduction of the a- and b-wave amplitudes persisted throughout the study. In conclusion, OCT can reflect early ultrastructural changes of photoreceptors manifesting as disrupted EZ and ELM prior to overt morphologic changes in histologic sections. In addition, the degree of changes in the EZ and ELM on OCT might predict the severity of impairment of photoreceptors.

Student Number : 2012-30271

Contents

viii

List of Tables

List of Figures

NaIO$_3$ administration. Hematoxylin and eosin (H&E)-stained retinal sections at baseline (H) and at days 2 (I), 7 (J) and 28 (K).

Figure 3-7. Histologic correlations with optical coherence tomography (OCT) images in 0.2mg sodium iodate (NaIO$_3$)-treated rabbits. Representative OCT images at baseline (A) and at days 1 (B), 2 (C), 4 (D), 7 (E), 14 (F) and 28 (G) after NaIO$_3$ administration. Hematoxylin and eosin (H&E)-stained retinal sections at baseline (H) and at days 2 (I), 7 (J) and 28 (K).

Figure 3-8. Histologic correlations with optical coherence tomography (OCT) images in 0.4mg sodium iodate (NaIO$_3$)-treated rabbits. Representative OCT images at baseline (A) and at days 1 (B), 2 (C), 4 (D), 7 (E), 14 (F) and 28 (G) after NaIO$_3$ administration. Hematoxylin and eosin (H&E)-stained retinal sections at baseline (H) and at days 2 (I), 7 (J) and 28 (K).

Figure 3-9. Histologic correlations with optical coherence tomography (OCT) images in 0.8mg sodium iodate (NaIO$_3$)-treated rabbits. Representative OCT images at baseline (A) and at days 1 (B), 2 (C), 4 (D), 7 (E), 14 (F) and 28 (G) after NaIO$_3$ administration. Hematoxylin and eosin (H&E)-stained retinal sections at baseline (H) and at days 2 (I), 7 (J) and 28 (K).

Figure 3-10. The serial changes of a- and b-wave amplitudes after intravitreal sodium iodate (NaIO$_3$) administration in rabbits. (A) 0.1-mg NaIO$_3$ group. (B) 0.2-mg NaIO$_3$ group. (C) 0.4-mg NaIO$_3$ group. (D) 0.8-mg NaIO$_3$ group.

◆ Note

Some parts of this dissertation are extracted and adapted from the journal publications which were published or submitted during the course of this study:

So Hyun Bae, Joonsoo Jeong, Sung June Kim, Hum Chung, Jong-Mo Seo. Investigation of Surgical Techniques for Optimization of Long-Term Outcomes of LCP-Based Retinal Prosthesis Implantation. Transl Vis Sci Technol 2018;7(4):17.

So Hyun Bae, Bum-Joo Cho, Hum Chung, Jong-Mo Seo. Anatomic correlations with retinal changes seen on optical coherence tomography in sodium iodate-induced retinal degeneration. Jpn J Ophthalmol. submitted, 2018.

Chapter 1: Introduction

1.1.　Retinal prosthesis

1.1.1.　Concept of retinal prosthesis

The photoreceptors in a healthy retina transform photons from light into electrical signals. Then the signals are carried through the bipolar cells and ganglion cells and propagate along the optic nerve to the visual cortex. Numerous patients affected by retinitis pigmentosa (RP) or age-related macular degeneration (AMD) lose their vision due to progressive deterioration of photoreceptors and retinal pigment epithelium (RPE) of the outer retina (Fig. 1-1). There is no established cure for RP or AMD and the most treatment modalities focused to slow down the progression of diseases. While, several studies had shown that abundant inner retinal neurons, comprising bipolar cells, amacrine cells and the retinal ganglion cells, survived in the macula despite near-total loss of photoreceptors in RP or AMD postmortem eyes.[1,2] The concept of retinal prostheses are based on the assumption as follows; the process of phototransduction in photoreceptors can be replaced by electrical current and the electrical stimulation to remnant inner retinal neurons can elicit some visual perception in blind patients due to outer retinal degeneration.[3]
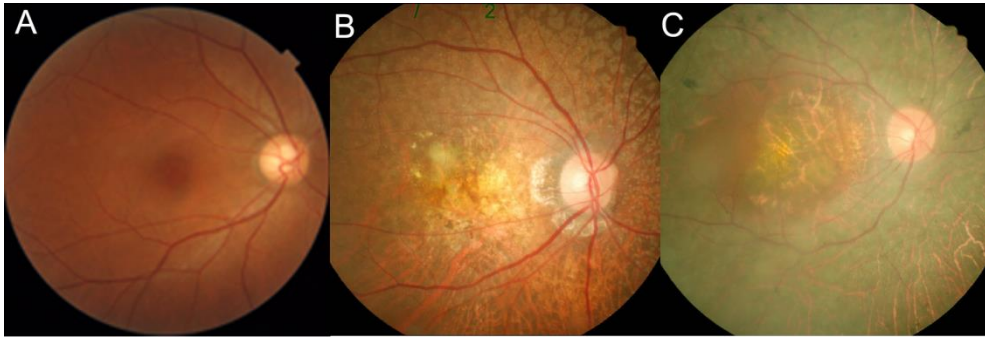
Figure 1-1. Fundus photographs of normal eye (A), age-related macular degeneration (B) and retinitis pigmentosa (C).

1.1.2. Basic components of retinal prosthesis

The basic components of prosthetic device consist of a light-capturing unit, electronics which transduce the captured image into electrical signal and an electrode array for stimulation of the remaining cells in the inner retina. The prosthetic device can use an external camera or photodiode array to detect the light. The photodiode array can detect light and transfer charge to the retina without the need for cameras.

The retinal prosthesis, consequentially, is based on a hybrid combination of a polymer-based electrode array and an extraocular electronics encapsulated in a hermetic package. The extraocular components of the retinal prosthesis comprise a connecting cable and a hermetic package that contains electronics including a receiver coil that couples with an external coil for power supply and signal transmission through wireless electromagnetic transfer.

2

1.1.3. Liquid crystal polymer-based retinal prosthesis

In current retinal prosthesis, most hermetic packages are made of metal or ceramic for good mechanical stabilization and biocompatibility with the human body. However, their bulky and heavy properties might compromise the long-term safety of prosthetic devices. In addition, its manufacture requires manual work resulting in high production cost and feedthroughs which might limit the density of stimulating electrodes. Recently, liquid crystal polymer (LCP) has been increasingly recognized as a new biocompatible material for neural prosthesis. LCP has several favorable properties for long-term implantable neural prosthesis such as low gas permeability compatible to that of glass[4] and lower water absorption compared to conventional polyimide and silicone elastomers.[5] Our group has developed and manufactured a seamless LCP-based monolithic retinal prosthesis by integrating its components (i.e., inductive coil, circuit, electrode array) on a single body of multilayered LCP films.[6] The monolithic fabrication allows miniaturization and a low-cost manufacturing process without the need of feed-through technology. Our group manufactured thin and light prosthetic device which fits the curved surface of the eyeball of human.[7, 8]

1.1.4. Current approaches for surgical implantation of electrode array

The electrode array is implanted into the eyeball to stimulate residual retinal neurons at different levels including epiretinal,[9,10] subretinal,[11-13] and

3

suprachoroidal sites.[14,15] Several multicenter clinical trials have shown that the epiretinal[10] and subretinal[11,13] implants were relatively well tolerated and restored some vision in nearly or completely blind patients. However, those approaches still have several risks associated with surgical procedures. Epiretinal implantation requires insertion of retinal tack to stabilize an electrode array on the epiretinal surface. The retinal tack penetrates the retina and choroidal tissue which might results in further damage and gliosis in already diseased retina.[16] In addition, several complications have been reported in the clinical trial using epiretinal implant including tack dislodging, endophthalmitis and retinal detachment.[10] Subretinal implantation can provide stable mechanical fixation of electrode array without the need of retinal tack insertion. However, the surgical techniques might be challenging to make the room for subretinal approach. The confined subretinal space may limit the device size. In addition, subretinal implantation may block the heat dissipation and supply of nutrients to the retina. The risks associated with subretinal implantation include loss of residual photoreceptors in already diseased retina, retinal detachment and retinal perforation due to surgical trauma.[17,18] In addition, conjunctival erosion and dehiscence have frequently appeared over packages or connecting cables in worldwide trials.[10,18] Suprachoroidal implantation provides mechanically stable fixation of electrode and allows less invasive surgical techniques without the need for pars plana vitrectomy or penetration of neural retina. However, there is still the risk of bleeding and retinal damage related to device implantation.[14] The overview of current retinal prosthetic devices of worldwide groups are shown in Table 1. The summary of advantages and

4

disadvantages of each surgical approach of retinal prosthesis is shown in Table 2.

1.1.5. Development of reproducible and safe surgical techniques for LCP-based retinal prosthesis

The reproducible and safe surgical techniques are essential prerequisite for the successful realization of retinal prosthesis. Retinal prosthesis implantation surgery, intraocular placement of the electrode array especially, requires high-level surgical skills to avoid damage to the diseased retina and achieve stabilization of the implanted device components. The establishment of reliable and reproducible surgical procedures ensuring the long-term safety of the prosthesis remains a challenge.

Table 1. Overview of current retinal prosthetic devices

Trial	Electrode array		Electronic package		
	Material	Placement	Material	Placement	Type of connection
Argus II[19]	Polyimide	Epiretina	Titanium	Sclera	Wireless
Epi-RET3 IOL Prosthesis[20]	Polyimide	Epiretina	Polyimide encapsulated with silicone	Intraocular (posterior chamber)	Wireless
Alpha-AMS[11]	Silicon-based photodiode on polyimide	Subretina	Ceramic	Retro-auricular	Wireless
Boston Retinal Implant Project[21]	Polyimide	Subretina	Titanium	Sclera	Wireless
Bionic Vision Australia[14]	Silicone	Supra-choroid	Titanium	Retro-auricular	Percu-taneous connector
NIDEK Visual Prosthesis[15]	Silicone	Supra-choroid	Titanium	Temporal bone	Wireless

Table 2. Summary of advantages and disadvantages of anatomic locations for electrical stimulation by retinal prostheses

Surgical approach	Advantage	Disadvantage
Epiretina	· Relatively easy surgical technique · Heat dissipation through the vitreous	· Need for retinal tack penetrating the retina · Need for vitrectomy · Risk of gliosis · Electrical stimulation to ganglion cells
Subretina	· Stable fixation without the need for retinal tack · Electrical stimulation to bipolar cells utilizing remaining retinal processing network	· Difficult surgical procedures · Need for vitrectomy · Need for incision into the retina · Limited transport of nutrients and oxygen from choroid to retina · Limited size of prosthetic device
Suprachoroid	· Easier and less invasive surgical technique without need for manipulation of retina itself · Stable fixation without the need for retinal tack · Heat dissipation through choroid · No obstacle for choroidal circulation	· Risk of intraocular bleeding · Longer distance between electrode and retina

1.2. Experimental retinal degeneration

1.2.1. Sodium iodate

Animal models of retinal degeneration have been important tools to understand the underlying pathophysiology and to develop novel therapies for retinal degenerative diseases such as AMD or RP. Sodium iodate ($NaIO_3$), an oxidizing agent, has been widely used to induce retinal degeneration in *in vitro* and *in vivo* experiments. $NaIO_3$ is known to affect the RPE selectively resulting in subsequent degeneration of photoreceptors.[22] While, recently, several studies have shown that $NaIO_3$ could induce direct damages to intraretinal neurons.[23,24] Time- and dose-dependent retinal changes after systemic administration of $NaIO_3$ have been reported in several reports.[25,26] In addition, the course of retinal degeneration induced by monocular intravitreal injection of $NaIO_3$ has been shown in rabbits.[27]

1.2.2. Assessment tools for retinal structural changes in retinal degeneration

In vivo evaluation of the structural changes of retina is important for understanding the development and progression in retinal degenerative diseases. Currently, optical coherence tomography (OCT) is the most widely used tool for *in vivo* evaluation of the retinal architecture. The significant advance of OCT technology has allowed delineation of multiple retinal layers, especially of the alternating outer retinal bands, which is to say the external limiting membrane (ELM), ellipsoid zone (EZ)

8

and RPE/Bruch's complex (Fig. 1-2).[28] Furthermore, the OCT instrumentation provides novel markers for early diagnosis and management of many retinal diseases,[29,30] thereby allowing for detection of ultrastructural changes of the retina, even in eyes with only subclinical changes. Current OCT-guided diagnosis and monitoring of diseases ultimately relies on accurate identification of the anatomic correlations of pathological changes in diseased eyes. A few studies have evaluated the correlations between OCT images and postmortem histology in animals and human donor eyes in order to understand the anatomic correspondences of retinal layers as shown on OCT.[31-34] However, information is still lacking on the anatomic correlations with abnormal OCT features in eyes with retinal degenerative diseases.
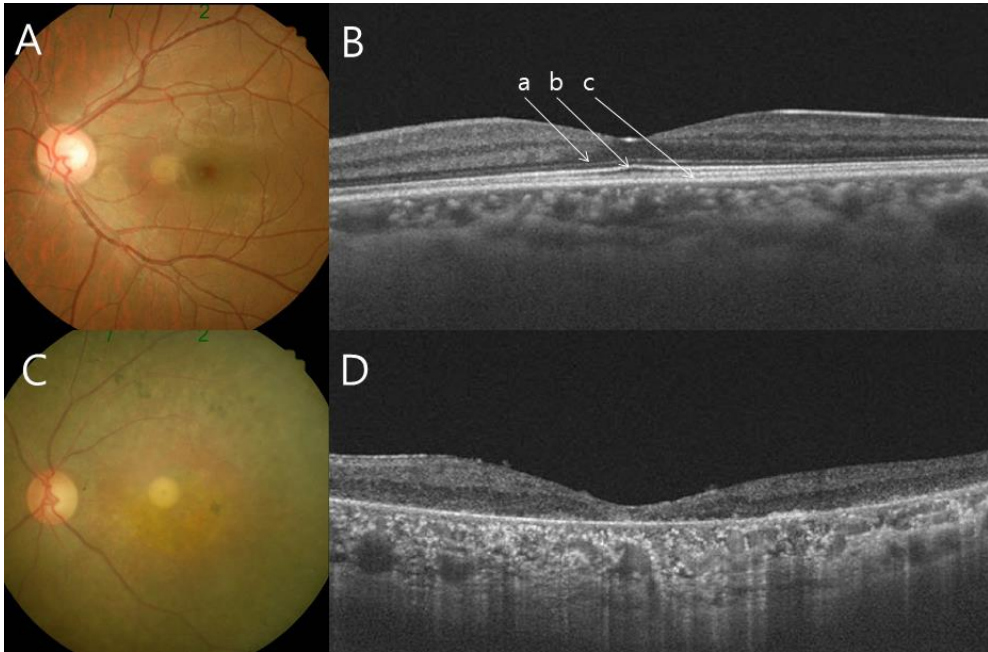
Figure 1-2. Fundus photographs and optical coherence tomography (OCT) in human. Fundus photographs of normal eye (A) and retinitis pigmentosa (C). (B) The OCT image of normal eye shows clear delineation of external limiting membrane (a), ellipsoid zone (b) and retinal pigment epithelium/Bruch's membrane complex (c). (D) The OCT image of retinitis pigmentosa shows marked disruption of outer retina with complete loss of external limiting membrane and ellipsoid zone.

1.3. Dissertation outlines

1.3.1. Establishment of optimized surgical procedures for implantation of LCP-based retinal prosthesis

This section contains the results about the investigation of basic surgical procedures for implantation of prototype LCP-based prosthetic device in the pilot study. Based on the experience of pilot study, we developed the reproducible surgical techniques to optimize the long-term safety of implantation surgery of the totally implantable LCP-based retinal prosthesis by *in vivo* experiments.

1.3.2. Anatomic correspondence with pathologic OCT features in experimental retinal degeneration

This section contains the experimental retinal degeneration after intravitreal injection of $NaIO_3$, followed by assessed by precise investigation of retinal structure and function using multiple tools including color fundus photographs, swept-source OCT (SS-OCT), histology and electroretinography (ERG). The intensive comparative analysis of data, as supported by ERG-based functional analysis, could provide clues to the histologic correlations of experimental retinal degeneration with abnormal OCT features. In this dissertation, we aimed to investigate the anatomic correlations with pathologic OCT features in experimental retinal degeneration induced by intravitreal $NaIO_3$ administration

Chapter 2. Methods

All of the procedures in this study were approved by the Animal Care and Use Committee of Seoul National University Hospital and adhered to the Association for Research in Vision and Ophthalmology (ARVO) Statement for the Use of Animals in Ophthalmic and Vision Research.

2.1. LCP-based retinal prosthesis

2.1.1. Pilot study

2.1.1.1. Prototype LCP-based prosthetic device

The design and fabrication method for the initial model of LCP-based prosthetic device has been developed by Lee et al.[35,36] Monolithically encapsulated LCP-based system was fabricated using photolithography of evaporated gold film and thermal-press bonding of multilayered LCP films to seal the electronics. The system package provides the hermetic enclosure for the electronic components such as a current stimulator ASIC, resistors, capacitors and telemetry coils. Thin gold layer was deposited on the LCP substrate of electrode array. The electrode array is connected to the package via the interconnection cable. The interconnection cable has a curved shape to minimize the irritation of overlying tissue and to avoid the bending of device itself during implantation surgery. The

fabricated package has a maximum thickness of 3 mm and a diameter of 23 mm.

The thickness of electrode array was 50 μm.[36] The mockups of prototype prosthetic

device is shown in Fig. 2-1.
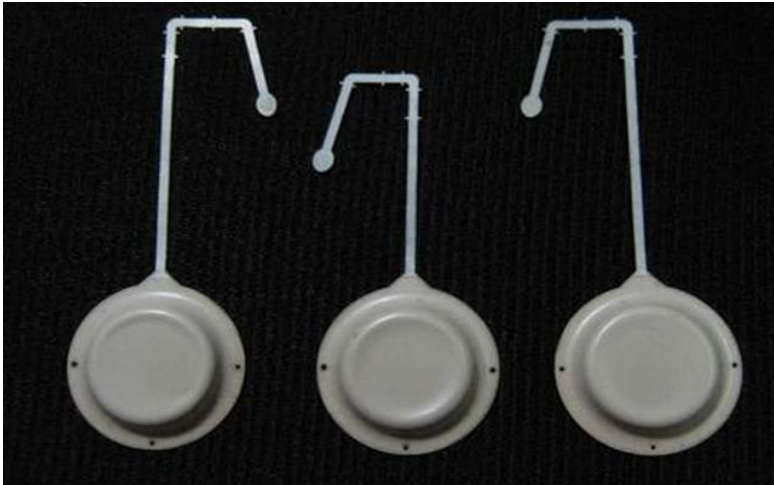
Figure 2-1. Mockups of prototype LCP-based retinal prosthetic device (This image
is quoted from Ph.D. dissertation of Lee[36])

2.1.1.2. Surgical techniques for implantation of prototype prosthetic device

Healthy adult New Zealand white rabbits aged 8 weeks were used in this study.

They were anesthetized by intramuscular injection of tiletamine/zolazepam (Zoletil;

Carros, France) and xylazine (Rompun; Bayer AG, Germany) in a 1:1 mixture at a

dose of 0.6 mL/kg. The mockups of LCP-based prosthetic device including the electrode array and system package were prepared for the implantation surgery. Before surgery, the eyelids, ocular surfaces and scalp were prepared with povidone-iodine solution, and the overall system was soaked in 70% ethanol and rinsed with sterile saline.

Two eyes of 2 rabbits were operated. The skin in the midline of the head was incised. The underlying subcutaneous tissue and muscle was carefully prepared and retracted to expose the skull from bregma and lambda. Then the fornix-based superior conjunctival peritomy was conducted from 10 o'clock to 2 o'clock. The subconjunctival pocket was deepened bluntly in the superotemporal quadrant of the eyeball and the superior retractor bulbi muscle was left without any manipulation. Then, the subcutaneous periorbital tissue and temporalis muscle were bluntly dissected to make a tunnel from the subconjunctival space to the surface of the skull. The package was positioned on the surface of the skull. The curved interconnection cable with electrode array was passed through the tunnel under the temporalis muscle and subcutaneous tissue. Then it was pulled into the subconjunctival space. Full-thickness scleral incision was made at least 3 mm from the corneal limbus posteriorly in the superonasal quadrant using a crescent knife (Sharptome 74-1010; Surgical Specialties Co., Reading, PA, USA). The electrode array was inserted into the suprachoroidal space and gently advanced posteriorly to reach the visual streak. The path of electrode array was monitored under panfunduscopic examination using a wide-field contact lens (Quad Pediatric; Volk

Optical Inc., Mentor, OH, USA). The interconnection cable was anchored onto the scleral surface using interrupted vicryl sutures. The conjunctival wound was repaired using interrupted vicryl sutures. The surgical wound of the scalp was closed over the package in layers using interrupted sutures of black silk and vicryl. However, contrary to other research groups,[37, 38] I did not use any additional sutures or bone screws to fix the package on the skull. After completion of the surgery, topical antibiotics (moxifloxacin 0.5%) and corticosteroid (prednisolone acetate 1%) were applied to the operated eye postoperatively for 1-2 weeks. A representative case of implantation surgery is shown in Fig. 2-2.

2.1.1.3. Assessments of biocompatibility and safety after surgery

The outcome of chronic implantation was investigated by inspection of scalp and anterior segment of the eyeball under microscope, color fundus photographs and spectral-domain OCT (Cirrus OCT, Carl Zeiss Meditec, Dublin, CA, USA). The scan protocols of Cirrus OCT included five-line raster scans across the tip of the electrode array. The position of system package was assessed by the skull x-ray projections.
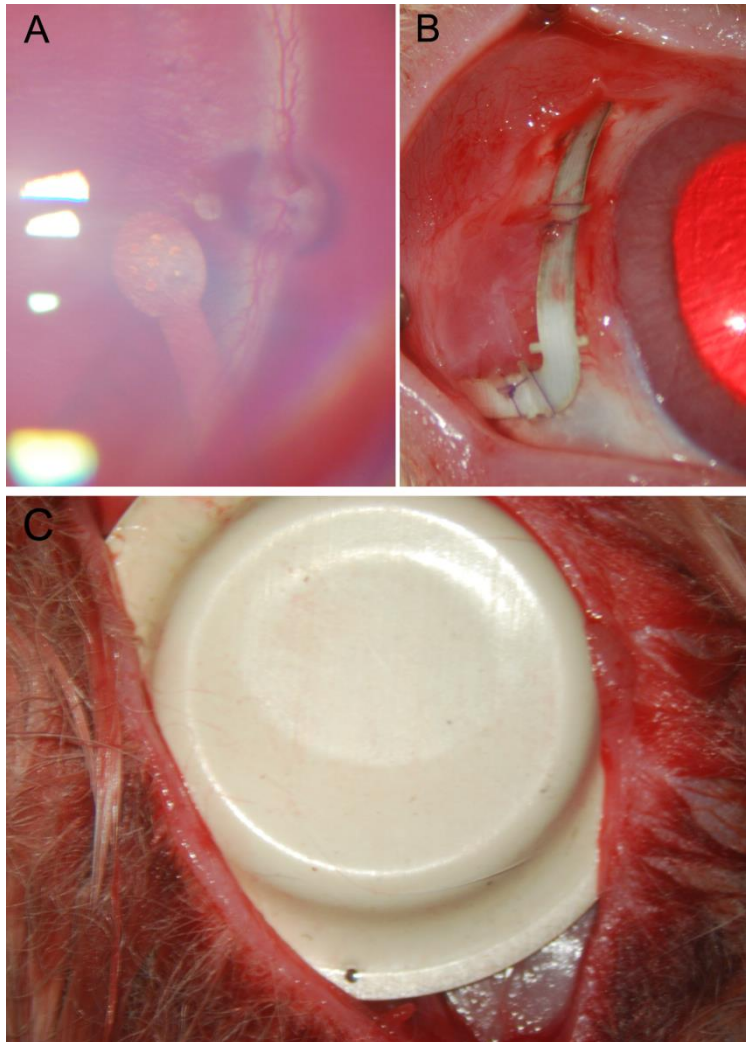
Figure 2-2. Intraoperative photographs of implantation surgery for prototype LCP-based prosthetic device. (A) The electrode array is successfully implanted into the suprachoroidal space. (B) The curved interconnection cable is fixed onto the sclera using interrupted sutures. The interconnection cable is connected to system package through the subconjunctival space and periorbital tissue. (C) The system package in placed on the skull after the incision of scalp.

2.1.2. Totally implantable LCP-based retinal prosthesis

2.1.2.1. Totally implantable LCP-based retinal prosthesis

The design and fabrication method for the modified version of LCP-based prosthetic device has been developed by Jeong et al.[6,39] The implanted components of the LCP-based retinal prosthesis consist of a circular package, an electrode array, and a transition part between the package and the electrode array (Fig. 2-3). The device with all of its components is fabricated monolithically on a single-body LCP substrate.[5,8,39] The device's overall design is streamlined for attachment to the curved eyeball surface. The circular package, of an eye-conformable structure resulting in a crescent-shaped cross-section as shown in Jeong et al,[39] has a maximum thickness of 1.3 mm and a diameter of 14 mm.[39] The electrode array, as formed by a laser-thinning process, has a thickness of 30 μm.[39,40] The maximal

width of electrode array was 3 mm. The transition part is deflected to connect the electrode array with the package. The complete unit of the device encases the planar receiving coil and current stimulator with electronic circuits. However, in this study, I used mockup devices that are physically identical to the complete unit, but lacking any embedded components. The specifications of the mockup devices were varied as follows; electrode array length ranging from 16 to 22 mm, transition part angle ranging from 60 to 70° and suturing holes along the anterior or posterior margin of package or transition part.
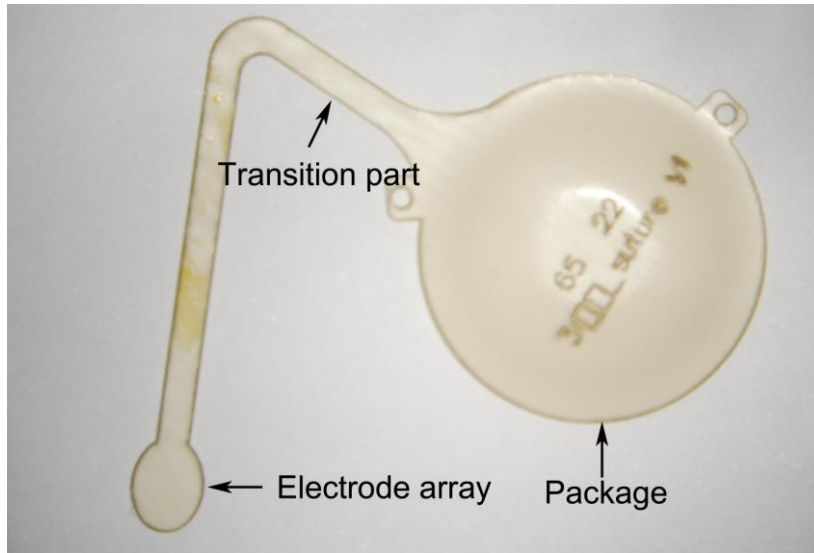
Figure 2-3. Mockup of totally implantable LCP-based retinal prosthetic device.

2.1.2.2. Surgical procedures for implantation of prosthetic device

Healthy adult New Zealand white rabbits aged 8 weeks were used in this study. They were anesthetized by intramuscular injection of tiletamine/zolazepam (Zoletil) and xylazine (Rompun) in a 1:1 mixture at a dose of 0.6 mL/kg. Before surgery, the eyelids and ocular surfaces were prepared with povidone-iodine solution, and the overall system was soaked in 70% ethanol and rinsed with sterile saline.

A total of 11 eyes of 11 rabbits were operated on for implantation of the LCP-based retinal prosthesis. After induction of anesthesia, fornix-based superior conjunctival peritomy was performed. In each experiment, I simulated where to fix the package and to make an incision to access the suprachoroidal space. Fornix-

based scleral tunneling (4 mm x 2 mm) was performed at least 3 mm from the corneal limbus posteriorly in the superonasal quadrant using a crescent knife. At the base of the scleral tunnel, a scleral incision was made to approach the suprachoroidal space. The configuration of the scleral incision is straight and parallel to the limbus and of a length of at least 4 mm. Prior to electrode-array insertion, the sclerotomy entrance was lubricated and each electrode was coated with viscoelastic substance such as Healon (Abbott Medical Optics, Santa Ana, CA, USA) or Viscoat (Alcon Laboratories, Fort Worth, Texas, USA). The electrode array was inserted into the suprachoroidal space without the aid of any guide foil. The advancement of the electrode array was carefully monitored under fundus examination with a wide-field lens (Quad Pediatric). I modified the path of the electrode array in order to position the fore part under the visual streak near the papilla. If the path of the electrode array was inadequate, the array was retracted and reinserted in the correct direction. The scleral incision was sealed with interrupted sutures, if needed. The package was placed deeply into the subconjunctival pocket in the superotemporal quadrant. It was anchored onto the sclera by interrupted sutures along its margin. The transition part between the package and the electrode array was attached to the sclera over the superior retractor bulbi muscle by several interrupted sutures in most cases except one. In one case (case 5), the transition part was passed under the superior retractor bulbi muscle after retraction of muscle. The conjunctiva was repaired with interrupted vicryl sutures. Subconjunctival injections of gentamicin were administered upon completion of the surgery. Topical antibiotics (moxifloxacin 0.5%) and

corticosteroid (prednisolone acetate 1%) were applied to the operated eye postoperatively for 1-2 weeks. A representative case of implantation surgery (case 8) is shown in Fig. 2-4.
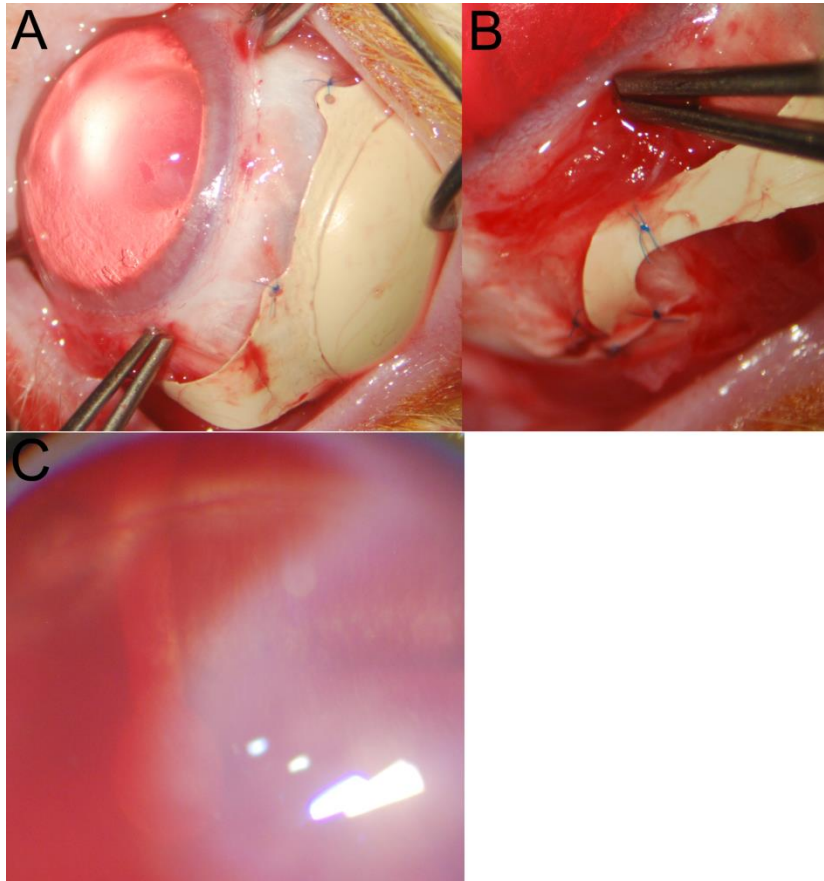
Figure 2-4. The details of surgical steps for implantation of modified LCP-based retinal prosthetic device. (A) The package is anchored onto the sclera with interrupted sutures. (B) The transition part is anchored onto the sclera and the sclerotomy is closed with interrupted sutures. (C) Fundus photograph shows suprachoroidally implanted electrode array without any complications such as retinal detachment or intraocular hemorrhage.

2.1.2.3. Assessment of safety during and after surgery

  The feasibility of each of the surgical steps was evaluated at the discretion of the surgeon. Additionally, the safety profile was assessed upon completion of the surgery and postoperatively. The fundus was carefully examined under a wide-field lens to confirm the presence of any intraocular hemorrhage, retinal tear or detachment, optic nerve damage or endophthalmitis. The anterior segment of the eyeball was inspected under operating microscope to detect any signs of infection, inflammation, conjunctival erosion or dehiscence, or cataract progression. Photographic images of the fundus and anterior segment of the eyeball were obtained regularly during the follow-up periods in order to evaluate any displacement of the device relative to certain ocular landmarks. Spectral-domain OCT (Spectralis OCT; Heidelberg Engineering, Heidelberg, Germany) was obtained across the tip of electrode implanted suprachoroidally.

2.2. Experimental retinal degeneration

2.2.1. Preparation of animals and $NaIO_3$ solution

Adult female New Zealand white rabbits aged 8 weeks were used in this study. They were anesthetized by intramuscular injection of tiletamine/zolazepam (Zoletil) and xylazine (Rompun). We prepared sterile solutions of $NaIO_3$ from solid $NaIO_3$ powder (Sigma-Aldrich, St. Louis, MO, USA) diluted in 0.9% normal saline. Four

different NaIO$_3$ solutions were prepared to obtain the dosages of 0.1, 0.2, 0.4, or 0.8mg in a volume of 0.05㎖ of solutions. Twenty rabbits were randomly assigned to 4 groups according to the dosages of NaIO$_3$ (n=5 for each group). The right eye of each rabbit received an intravitreal injection of a 0.05㎖ NaIO$_3$ solution according to assigned groups, while the left eye was left untreated. After intravitreal injections, topical antibiotics (moxifloxacin 0.5%) and corticosteroid (prednisolone acetate 1%) were applied to the operated eye postoperatively for 1-2 weeks.

2.2.2. Assessments of structural and functional changes of retina

The animals were assessed before (baseline) and after intravitreal NaIO$_3$ injections at days 1, 2, 4, 7, 14, 21, and 28. Ophthalmic examinations consisted of fundus photography, SS-OCT, ERG and histologic examinations. The pupils were maximally dilated by topical tropicamide 0.5% and phenylephrine hydrochloride 0.5% (Mydrin-P; Santen Pharmaceutical Co., Osaka, Japan).

2.2.2.1. Fundus photography and optical coherence tomography

The fundus was examined under a wide-field lens (SuperQuad® 160, Volk Optical, Inc., Mentor, OH, USA), and color fundus photographs were obtained with a digital camera (D60, Nikon Corp., Tokyo, Japan). Trained examiners acquired retinal cross-sectional images using SS-OCT (DRI OCT-1 Atlantis, Topcon Inc., Tokyo, Japan) under the 9-mm high-resolution volume-scan protocol. The outer

retinal hyper-reflective bands on SS-OCT images were referred to as the ELM, EZ and RPE/Bruch's membrane according to the International Nomenclature for Optical Coherence Tomography Panel.[28]

2.2.2.2. Electroretinography

Full-field ERGs were recorded monocularly in anesthetized animals. We used a hand-held multispecies ERG unit with mini-Ganzfeld (HMsERG; Ocuscience, Kansas City, MO, USA). An active electrode (ERG-jet, Fabrinal SA, Switzerland) was placed on the corneal surface after topical anesthesia with proxymetacaine hydrochloride 0.5% eyedrops (Alcaine, Alcon Laboratories Inc., Texas, USA). A reference electrode was attached to the occipital area, and a needle electrode was grounded in the ear. The animals were dark-adapted for more than 30 minutes before the test and dark-adapted 3.0 ERG was measured for maximal combined rod and cone responses.[41] The strength of stimulus was 3.0 photopic $cd \cdot s \cdot m^{-2}$. The stimulus duration was 3ms. The responses were amplified with a bandpass filter between to 0.3 and 300 Hz. Five responses recorded in an interval of 10 s were averaged using computer. The amplitude of the a-wave was measured from its baseline to its trough; the amplitude of the b-wave was measured from the a-wave trough to the b-wave's peak.

2.2.2.3. Histology

The eyeballs were enucleated at days 2, 7, and 28 after intravitreal $NaIO_3$ administration. They were fixed in 10% formalin and dissected across the visual

streak. One half of the eyeball was embedded in paraffin. Then, 5-μm-thick sections were obtained and stained with hematoxylin and eosin (H&E). The pathologic changes of each retinal layer were assessed under light microscopy (BX-50, Olympus Corp., Tokyo, Japan) and recorded with a digital camera.

2.2.3. Statistical analysis

Continuous variables are presented herein as the mean ± standard deviation (SD), and categorical variables are given as numbers or percentages. The ERG data at each time point was compared with the baseline using the paired t-test. Statistical analyses were performed using SPSS software version 24.0 (IBM-SPSS, Chicago, Illinois, USA). Results with a P value < 0.05 were considered statistically significant.

Chapter 3. Results

3.1. LCP-based retinal prosthesis

3.1.1. Pilot study

The implantation surgery was successfully conducted without any damages of eyeball and scalp in 2 rabbits. We regularly monitored the status of implanted retinal prosthesis for 8 months in one rabbit and for 10 months in the other. Fundus photographs confirmed the successfully implanted electrode array in the suprachoroidal space without any complications such as retinal detachment or intraocular hemorrhage in both rabbits (Figs. 3-1A, B). There were no complications in the anterior segment of eyeball such as inflammation, infection or conjunctival erosion/dehiscence (Fig. 3-1C). The cross-sectional OCT images showed that the tip of electrode array was positioned properly in the suprachoroidal space without any deformation of retina or choroid in two rabbits (Figs. 3-2A, B). The lateral view of skull x-ray showed that the system package was positioned adequately on the skull in both rabbits (Figs. 3-2C). The position of electrode array and system package was maintained without any displacement of the devices during the follow-up period up.
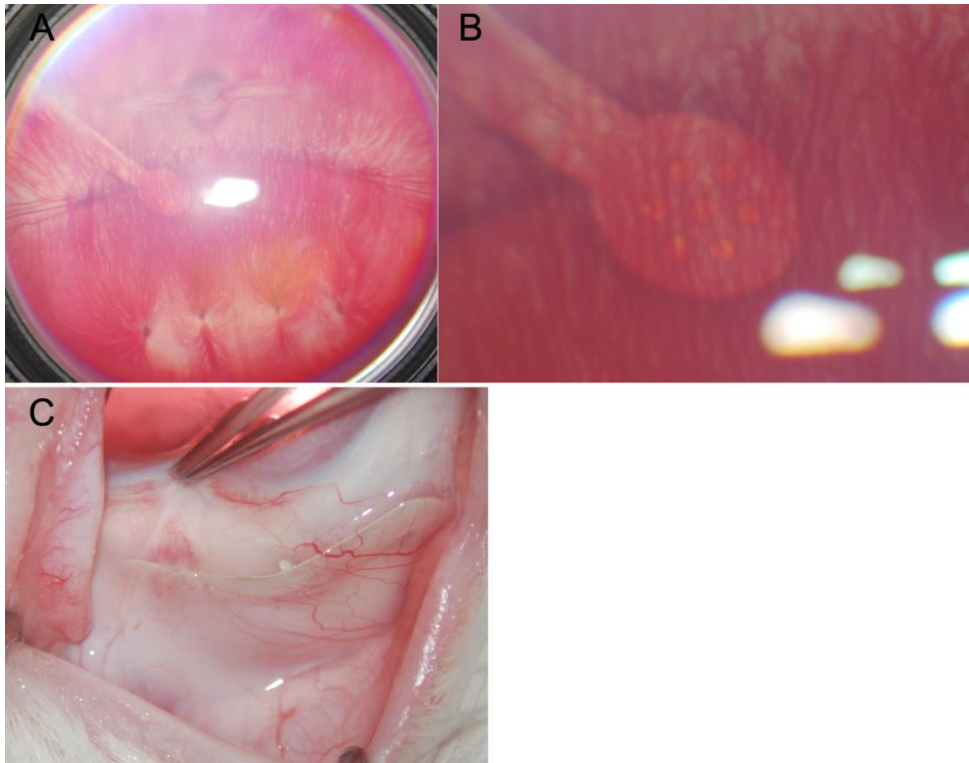
Figure 3-1. Photographs of fundus and anterior segment of implanted prototype retinal prosthesis at 10 months after implantation surgery. (A) Suprachoroidally implanted electrode array with an optimal position under the visual streak. (B) Magnified views of suprachoroidally implanted electrode array. (C) Implanted package on sclera without any inflammation or dehiscence of overlying conjunctiva.
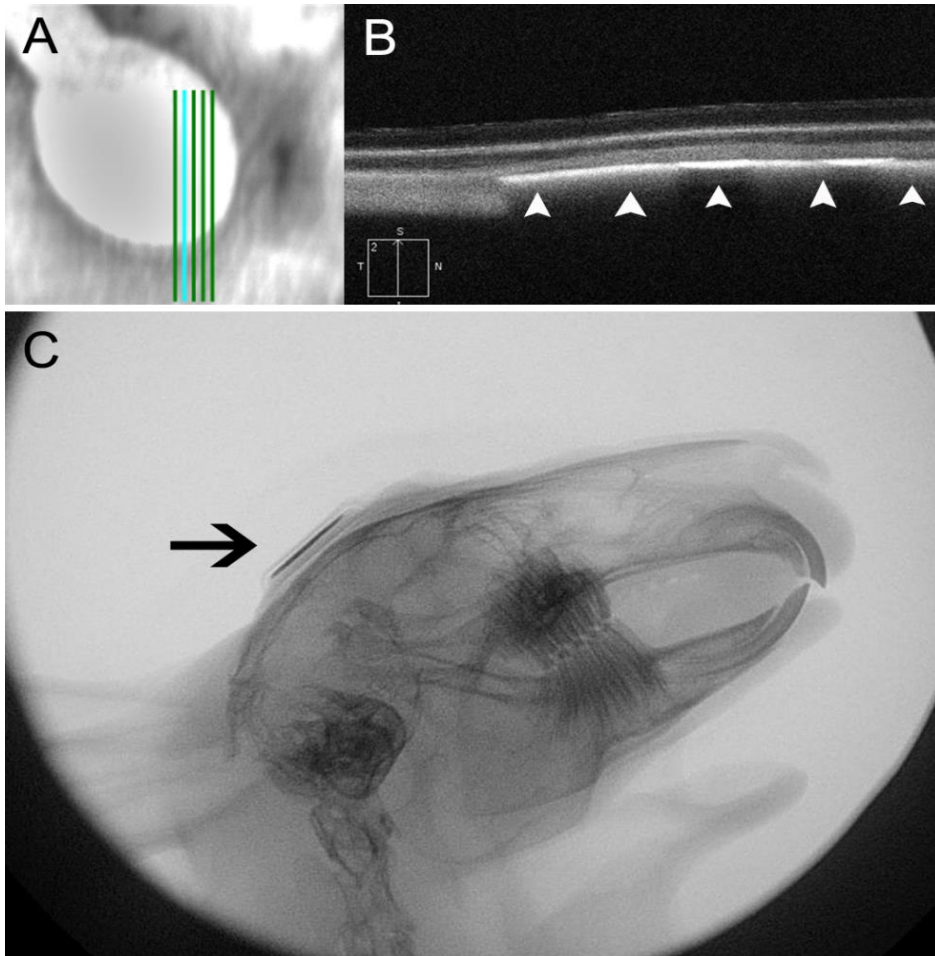
Figure 3-2. The images of optical coherence tomography (OCT) and x-ray of implanted prototype retinal prosthesis at 10 months after implantation surgery. (A) The blue line of infrared fundus image shows the direction of the OCT scan. (B) The cross-sectional OCT image represents successfully implanted electrode array (white arrowhead) in the suprachoroidal space without any damages of retina or choroid. (C) Lateral view of skull x-ray shows proper position of system package (black arrow) on the skull.

3.1.2. Totally implantable LCP-based retinal prosthesis

The surgical outcome of each case is summarized in table 3.

3.1.2.1 Implantation surgery

The surgical procedures for implantation of the modified prosthetic device were easily performed in 9 of 11 cases. With the exception of two cases (cases 5 and 10), there were no major intraoperative complications such as massive choroidal or subretinal hemorrhage, vitreous hemorrhage, or retinal detachment. The distance between the limbus and scleral incision ranged from 3 to 7 mm: 3 – 4 mm in 7 eyes (63.6%), 4 – 6 mm in 1 eye (9.1%), and over 6 mm in 3 eyes (27.3%). The sclerotomy sites were well-preserved without any significant bleeding during the scleral incision or insertion of the electrode array. The fundus examination under a wide-field lens clearly visualized the advancement of the electrode without any need of assistance by guiding foil. The tips of the electrode arrays were properly located under the visual streak near the papilla in 6 eyes (54.5%; Fig. 3-3A). In addition, the positions of the tips were acceptable in 3 eyes (27.3%; Figs. 3-3B, C); it did not reach the visual streak but only the medullary ray in 1 eye (9.1%, case 3), due to the short length (16 mm) of the electrode array; they passed through the visual streak by 1-3 disc diameters in 2 eyes (18.2%; cases 8, 9). The remaining 2 eyes showed inadequate electrode placement with surgical complications related to electrode insertion: optic nerve damage in 1 eye (case 5) and retinal tear in 1 eye (case 10). In case 5, the optic nerve was penetrated by the electrode array because I

had misjudged the course of insertion and the position of the package. In case 10, the retinal tear developed near the visual streak due to the excessive force exerted for advancement of the electrode array. In both of those cases, the scleral incision has been made more than 6 mm from the limbus. In all cases, the packages and transition parts were successfully anchored onto the scleral surface. The distance between the limbus and the anterior margin of the package ranged from 2.5 to 4 mm.
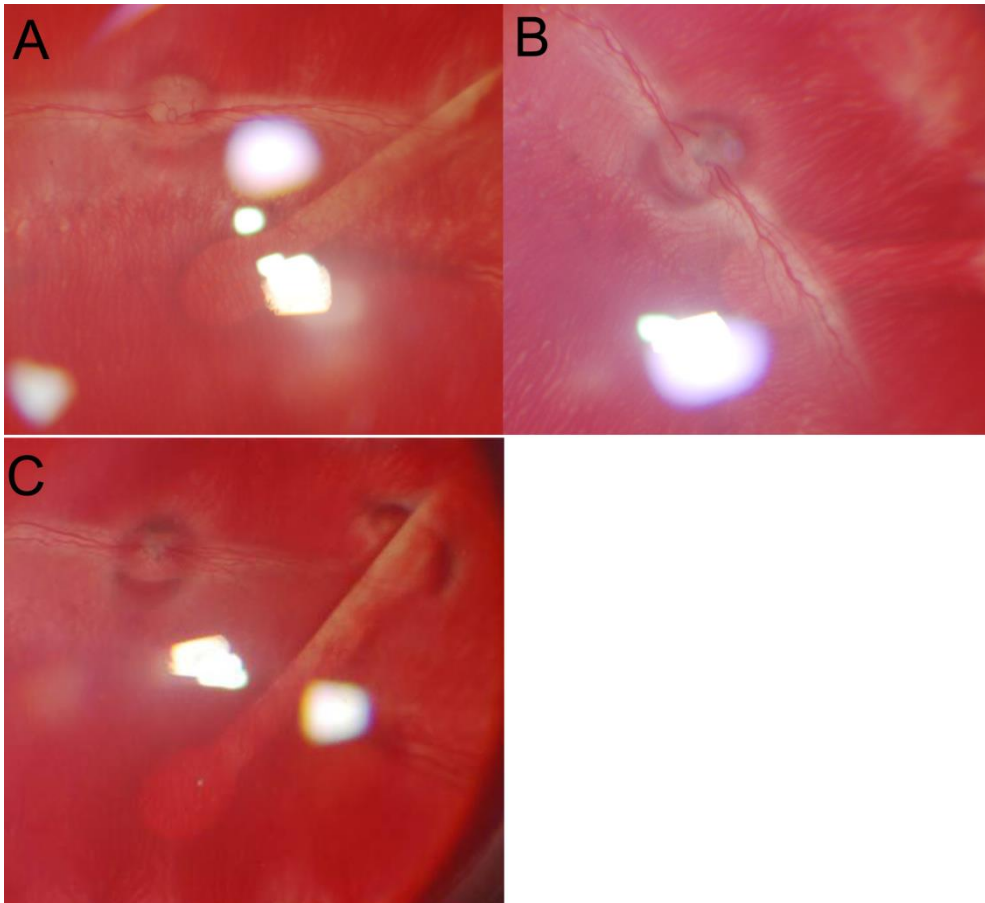
Figure 3-3. Position of suprachoroidally implanted electrode array. (A) The electrode tip is properly located under the visual streak. (B) The electrode tip is placed under the medullary ray due to the short length of the electrode array. (C) The electrode array passes through the visual streak due to the improper position of the scleral incision.

3.1.2.2. Postoperative assessments

In all cases except one, the devices were safely implanted in the eyeball for at least 3 months. In that one exceptional case (case 9), the surgeon found out extreme redundancy of transition part due to malposition of device during surgery. The surgeon had tried to attach the transition part to the scleral surface by anchoring sutures to minimize the bulging of that part but failed. The protruded portion of the transition part eventually resulted in conjunctival dehiscence and displacement of the package by one month postoperatively. Over the 3-month period, in most cases, there appeared to be two crucial complications related to the extraocular components of the devices: exposure of the package or of the transition part. Conjunctival erosion or dehiscence over the transition parts was detected in 4 cases: 2 cases at 4 months (cases 2 and 7) and 2 cases at 10 months postoperatively (cases 3, 11; Fig. 3-4). Conjunctival dehiscence over the package was shown in 5 cases: 4 cases at 6 months (cases 1, 4, 8, 10) and 1 case at 8 months (case 6). The packages began to be pushed forward and rotated gradually, followed by detachment of the fixation sutures. This resulted in excessive tension of the overlying conjunctiva along the anterior margin of the package, which in turn induced the conjunctival dehiscence and displacement of the package. In those cases, the transition part passed over the superior retractor bulbi muscle and directly contacted the overlying conjunctiva. However, in one case (case 5), the transition part was attached to the sclera under the retractor bulbi muscle and was maintained without any conjunctival erosion or dehiscence over the course of 1 year. No signs of infection

related to the device were detected prior to the development of conjunctival erosion or dehiscence over the external components of the prosthesis.

The fundus examinations revealed that in general, the electrode arrays in the suprachoroidal space were well tolerated without any significant postoperative complications such as intraocular inflammation, hemorrhage or array drift, regardless of the postoperative status of the extraocularly implanted components. The OCT images confirmed the proper positioning of the implanted electrode arrays in the suprachoroidal space. The representative case with postoperative OCT image is shown in Fig. 3-5. However, optic nerve or retinal damage continued to progress in the two aforementioned cases of intraoperative electrode-related complications: in one eye (case 5), the electrode array was displaced into the vitreous cavity as the result of optic nerve penetration, and in the other eye (case 10), chorioretinal atrophy along the path of the electrode was gradually extended as the result of retinal tear, but without development of retinal detachment.
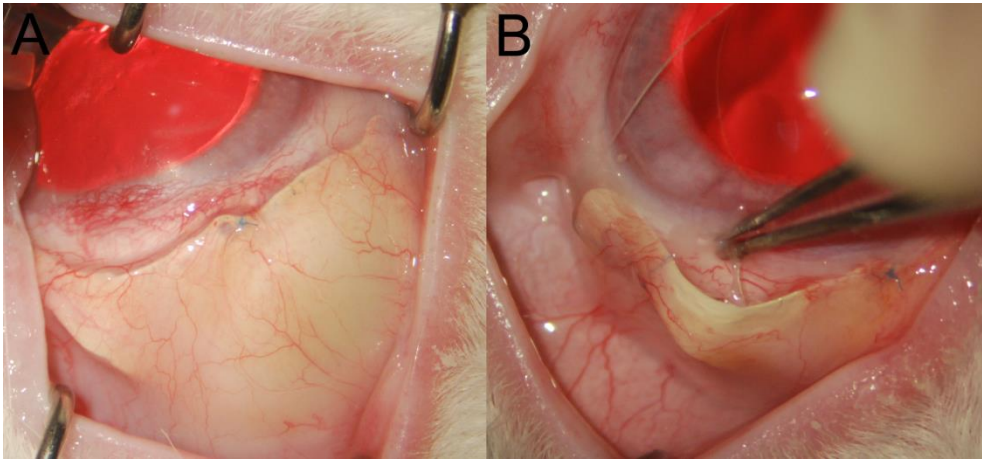
Figure 3-4. Anterior photographs of implanted retinal prosthesis package. (A) Implanted package on sclera with intact overlying conjunctiva 2 months after surgery. (B) Conjunctival dehiscence over transition part of implant 4 months after surgery.
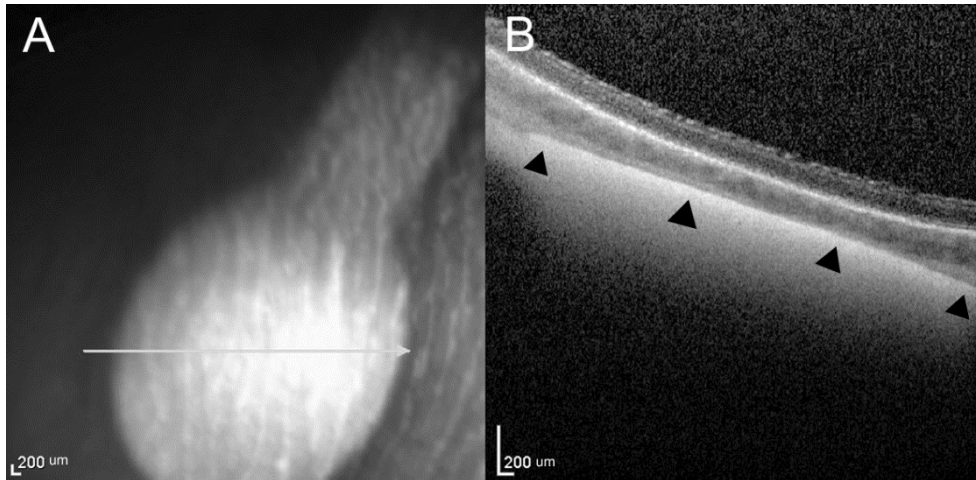
Figure 3-5. Representative optical coherence tomography (OCT) image of electrode array at 6 months after implantation surgery. (A) Infrared fundus image shows the location of electrode array. (B) Cross-sectional OCT image through the white arrow in (A) shows the normal retinal structure overlying the implanted electrode array. Black arrowheads indicate the suprachoroidally implanted electrode array.

Table 2. Summary of surgical outcomes for liquid crystal polymer-based retinal prosthesis

Rabbit No.	Scleral incision from the limbus tip	Position of electrode array	Intraoperative complication	Postoperative complication related to external component of device			Postoperative complication related to intraocular component of device	
				Onset	Type	Location	Onset	Type
1	3mm	Under visual streak	-	6 mo	Conjunctival erosion/dehiscence	Package		-
2	3mm	Under visual streak	-	4 mo	Conjunctival erosion/dehiscence	Transition part		-
3	3.5mm	Acceptable*	-	10 mo	Conjunctival erosion/dehiscence	Transition part		-
4	3.5mm	Under visual streak	-	6 mo	Conjunctival erosion/dehiscence	Package		-
5	6.5mm	Inadequate†	Optic nerve damage	12 mo	-		3 mo	Displaced electrode array
6	3.5mm	Under visual streak	-	8 mo	Conjunctival erosion/dehiscence	Package		-
7	3.5mm	Under visual streak	-	4mo	Conjunctival erosion/dehiscence	Transition part		-
8	5mm	Acceptable	-	6 mo	Conjunctival erosion/dehiscence	Package		-
9	6.5mm	Acceptable	-	1 mo	Conjunctival dehiscence	Transition part		-
10	6.5mm	Inadequate	Retinal tear	6 mo	Conjunctival erosion/dehiscence	Package	4 mo	Chorioretinal atrophy
11	3.5mm	Under visual streak	-	10 mo	Conjunctival erosion/dehiscence	Transition part		-

mo = months, - = none

*The tips of the electrode arrays were located within 3 disc diameters of the visual streak.

The tips of the electrode arrays were located over 3 disc diameters of the visual streak.

3.2. Experimental retinal degeneration

3.2.1. Comparative analysis of morphological changes of retina

3.2.1.1. Low-dose NaIO$_3$ group (0.1 and 0.2mg)

In the 0.1-mg group, each retinal layer was clearly identified with relatively normal architecture on OCT images throughout the course of the experiments (Fig. 3-6). The histologic examinations did not detect any structural changes of the retina until the end of the experiments. The outer retinal laminations including the ELM, EZ and RPE layers also were clearly delineated at each time point (Fig. 3-6).

In the 0.2-mg group, the reflectivity of the outer retinal layers including the EZ and ELM became altered as early as 2 days after NaIO$_3$ injection (Fig. 3-7C). At that time point, the overall intensities of the EZ and ELM were slightly lower relative to the baseline, though their integrities were relatively well-preserved (Fig. 3-7I). At 4 and 7 days, the changes of the outer retinal layers on OCT images had progressed slightly, showing an indistinguishable ELM and a slightly obscure EZ layer in two rabbits (50%) (Figs. 3-7D, E). By contrast, the histologic sections at 2 and 7 days revealed relatively well-organized and clearly-delineated retinal layers (Figs. 3-7I, J). At 14 days, the reflectivity of the outer retina on OCT images began to be recovered (Fig. 3-7F). At 28 days, the integrity and intensity of the EZ were restored to the baseline levels, while the intensity of the ELM did not reach the original level, showing a slightly lower overall contrast (Fig. 3-7G). Meanwhile, the histologic analysis at 28 days showed a normal retinal structure (Fig. 3-7K).

Figure 3-6. Histologic correlations with optical coherence tomography (OCT) images in 0.1mg sodium iodate (NaIO$_3$)-treated rabbits. Representative OCT images at baseline (A) and at days 1 (B), 2 (C), 4 (D), 7 (E), 14 (F) and 28 (G) after NaIO$_3$ administration. Hematoxylin and eosin (H&E)-stained retinal sections at baseline (H) and at days 2 (I), 7 (J) and 28 (K). Each retinal layer was clearly delineated in both OCT and histologic sections throughout the course of the experiment.

Figure 3-7. Histologic correlations with optical coherence tomography (OCT) images in 0.2mg sodium iodate (NaIO$_3$)-treated rabbits. Representative OCT images at baseline (A) and at days 1 (B), 2 (C), 4 (D), 7 (E), 14 (F) and 28 (G) after NaIO$_3$ administration. Hematoxylin and eosin (H&E)-stained retinal sections at baseline (H) and at days 2 (I), 7 (J) and 28 (K). The OCT images at day 4 (D) and 7 (E) showed an indistinguishable external limiting membrane and a slightly obscure ellipsoid zone despite the relatively well-organized retinal layers in the histologic sections.

3.2.1.2. Intermediate-dose NaIO$_3$ group (0.4mg)

In the 0.4-mg group, the outer retinal layers including the EZ and ELM became completely indistinguishable, having been replaced by a diffuse thick hyper-reflective zone on OCT images as early as 1 day after NaIO$_3$ injection in all rabbits (Fig. 3-8B). The reflectivity of the outer nuclear layer (ONL), which previously was a hypo-reflective band, appeared to increase, manifesting as a blurring of the boundary with the neighboring outer plexiform layer (OPL). Also, moderate swelling of the entire retina was observed, as accompanied by swelling of the retinal nerve fiber layer (RNFL) and ganglion cell layer (GCL).

At 2 days, the retinal swelling was slightly decreased, while the loss of the outer retinal laminations and the increased reflectivity of the ONL were persistent, on OCT imaging (Fig. 3-8C). The internal limiting membrane (ILM) was partially separated from the underlying retinal tissue in 3 rabbits (60%). At this time point, the histologic assessment indicated a slightly disorganized arrangement of the photoreceptor inner and outer segments (IS and OS); however, interestingly, the overall strata of the photoreceptor cell nuclei, IS and OS were relatively distinguishable (Fig. 3-8I). The photoreceptor cell nuclei in the ONL were relatively well-preserved, but the RPE cell nuclei were hardly visible. Contrastingly, the inner retinal layers including the inner nuclear layer (INL), inner plexiform layer (IPL) and GCL were relatively spared, with the exception of the partial detachment of the ILM.

At 4 days, the swelling of the retina and the reflectivity of the outer retina began to be reduced with persistent complete disintegration of the outer retinal laminations on OCT images (Fig. 3-8D). At 7 days, marked thinning of the entire retina, accompanied by prominent reduction of the outer retinal hyper-reflective zone, was detected (Fig. 3-8E). Meanwhile, the inner retinal layers including the INL, IPL and GCL were still visible. At this time point, the histologic examinations identified complete loss of RPE and photoreceptors including the photoreceptor nuclei, IS and OS, thus confirming the OCT results (Fig. 3-8J). The outer retina, previously occupied by photoreceptors, was filled with cellular debris, glial tissue and recruited cells (possibly macrophages) corresponding to the location of the outer hyper-reflective layer on OCT images. The structure of the INL was also irregular, showing a decreased number of cell nuclei in H&E-stained sections, though the overall laminations of the inner retina, including the GCL and INL, were still detectable on OCT images.

At 14 days (Fig. 3-8F), the thinning of the outer retinal hyper-reflective layer became more pronounced, followed by complete loss of the outer layer and subsequent thinning of the inner layer at 28 days (Fig. 3-8G). At 28 days, the histologic analysis showed further thinning of the entire retina, with a reduction of outer glial tissue and progressive loss of cell nuclei in the INL and GCL (Fig. 3-8K).
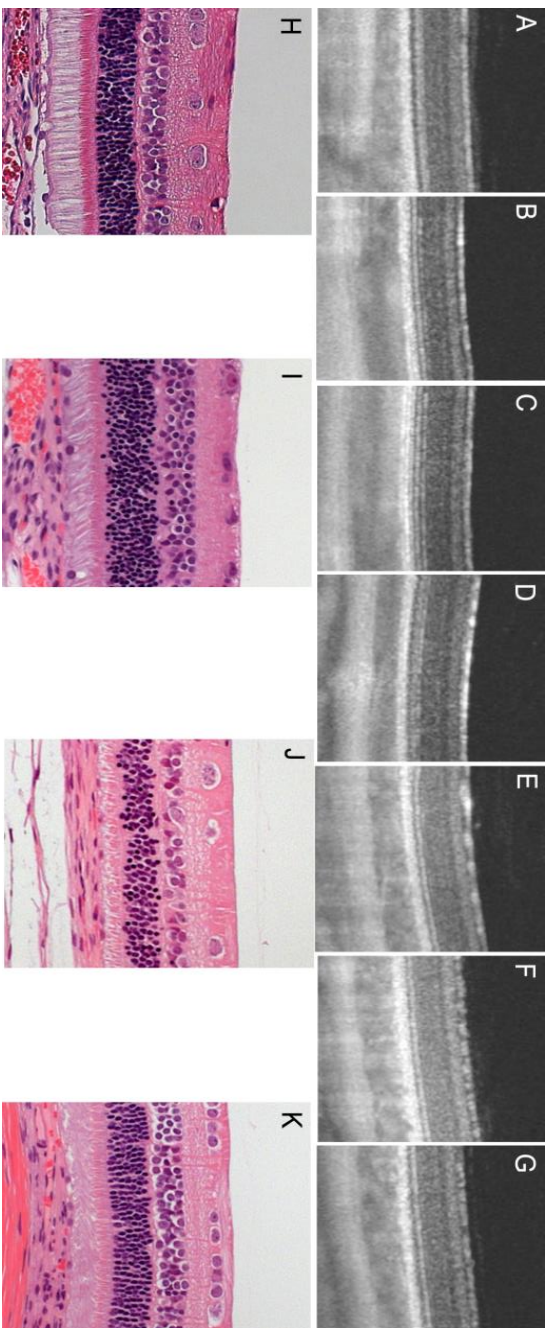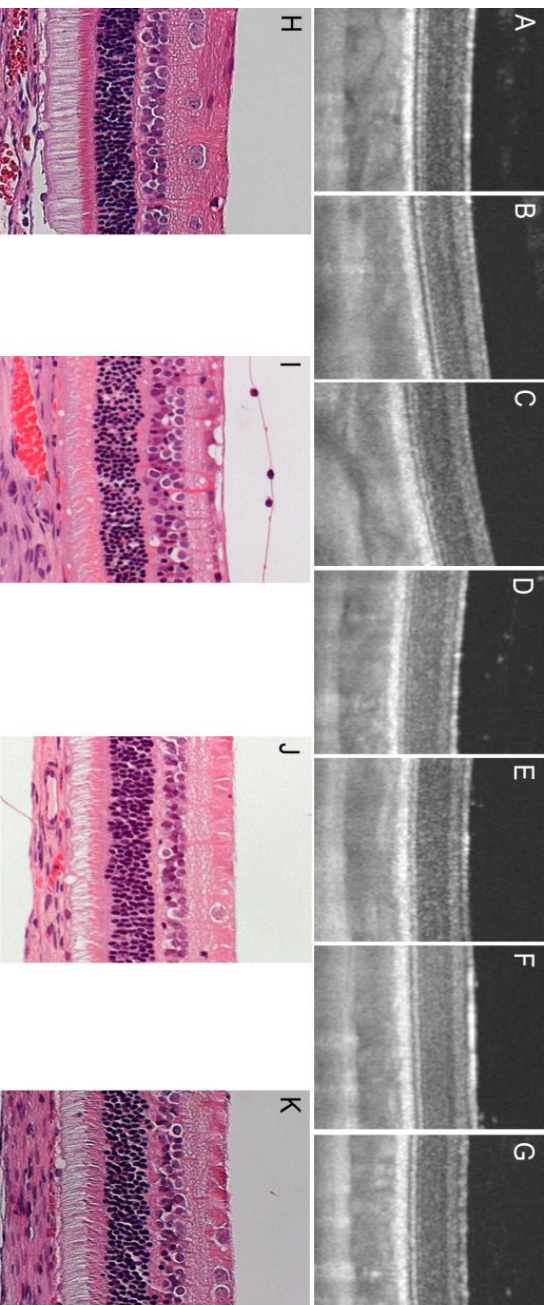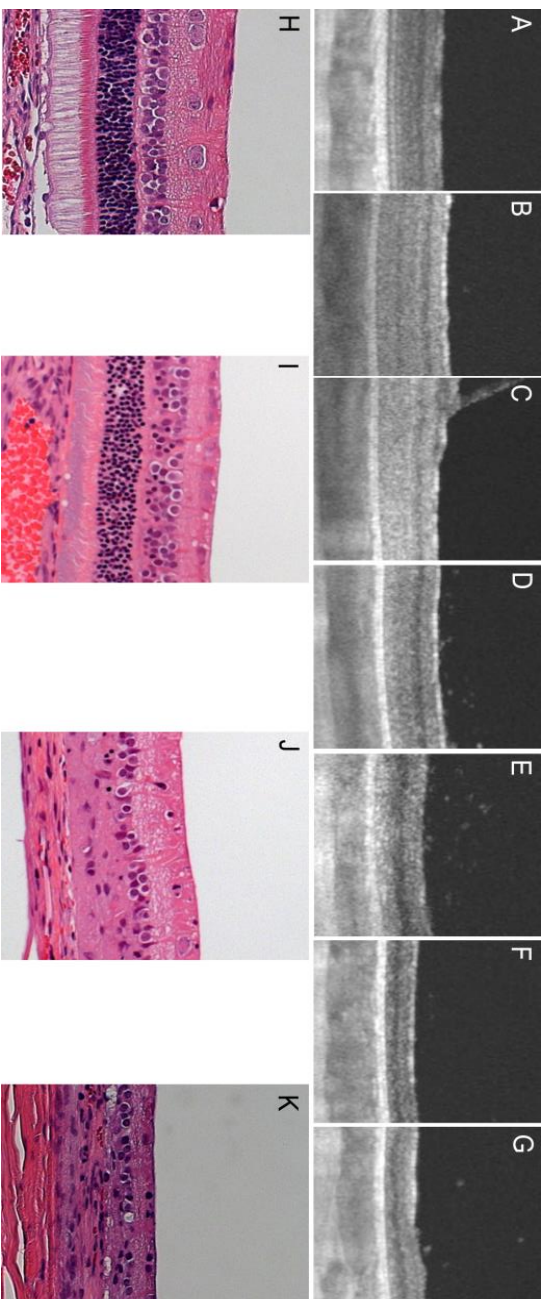
Figure 3-8. Histologic correlations with optical coherence tomography (OCT) images in 0.4mg sodium iodate (NaIO₃)-treated rabbits. Representative OCT images at baseline (A) and at days 1 (B), 2 (C), 4 (D), 7 (E), 14 (F) and 28 (G) after NaIO₃ administration. Hematoxylin and eosin (H&E)-stained retinal sections at baseline (H) and at days 2 (I), 7 (J) and 28 (K). The outer retinal laminations were lost on OCT images from day 1 (B) after NaIO3 injection. However, at day 2 (I), the overall strata of the photoreceptor cell nuclei and inner and outer segments were relatively distinguishable in the histologic section.

4 1

3.2.1.3. High-dose NaIO$_3$ group (0.8mg)

For the 0.8-mg group, the OCT images showed drastic retinal swelling accompanied by prominent swelling of the inner retina and loss of outer retinal laminations in all rabbits at 1 day after NaIO$_3$ injections (Fig. 3-9B). The ILM became detached from the underlying retinal tissue at 2 days (Fig. 3-9C). In the histologic analysis, the ILM also was separated, with extensive destruction of the inner retinal tissue including the GCL and INL, at 2 days (Fig. 3-9I). By contrast, the outer retinal layer including the photoreceptor nuclei, IS and OS remained relatively distinguishable, though the RPE cells were already hardly detectable. At 4 days (Fig. 3-9D), retinal atrophy began to progress, resulting in subsequent marked retinal thinning and completely indistinguishable retinal layers at 7 days (Fig. 3-9E). Consequently, after 14 days, the retinal tissue was hardly detectable on OCT images, complete retinal degeneration having occurred (Figs. 3-9F, G). In the histologic analysis, the entire retina was completely destroyed, leaving an almost-bare choroid after 7 days until the end of the study (Figs. 3-9J, K).
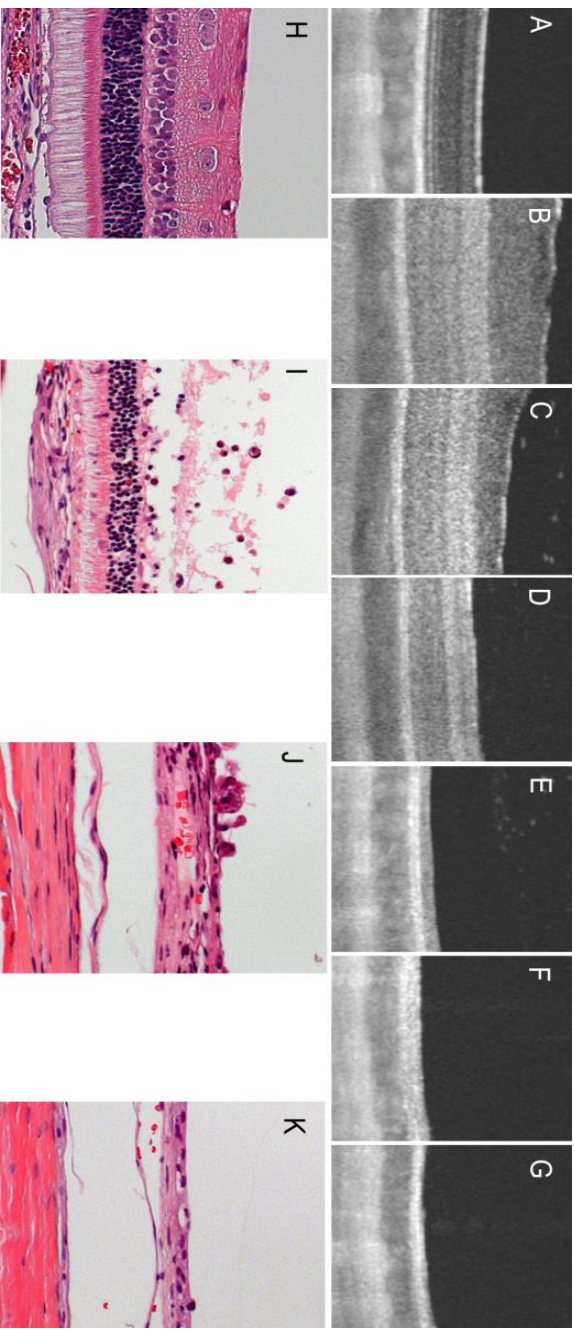
Figure 3-9. Histologic correlations with optical coherence tomography (OCT) images in 0.8mg sodium iodate ($NaIO_3$)-treated rabbits. Representative OCT images at baseline (A) and at days 1 (B), 2 (C), 4 (D), 7 (E), 14 (F) and 28 (G) after $NaIO_3$ administration. Hematoxylin and eosin (H&E)-stained retinal sections at baseline (H) and at days 2 (I), 7 (J) and 28 (K). Drastic retinal swelling on OCT (B, C) and prominent destruction of the inner retina in the histologic section (I) were followed by extreme retinal atrophy on OCT (E-G) and in the histologic sections (J, K).

3.2.2. Functional changes of retina

The changes of scotopic full-field 3.0 ERG responses at different time points after $NaIO_3$ injection are summarized in Fig. 3-10.

3.2.2.1. Low-dose $NaIO_3$ groups (0.1 and 0.2mg)

In the 0.1-mg group, there was no significant reduction of a-wave amplitude relative to the baseline throughout the follow-up periods, though a slight numerical reduction of a-wave amplitudes was shown from days 2 to 4 after $NAIO_3$ injection. Meanwhile, the 0.2-mg-treated rabbits showed numerical reduction of a-wave amplitudes from days 1 to 7 after $NaIO_3$ injection; also, the amplitudes of a-wave at days 2 and 4 were significantly decreased relative to those at the baseline ($P = 0.011$ and 0.025). These changes of a-wave in the 0.2-mg group appeared to be correlated with the altered reflectivity of the EZ on OCT images at those time points. After 14 days, the amplitudes of the a-wave were recovered to the levels of the baseline in both the 0.1- and 0.2-mg groups. Contrastingly, the amplitude of the b-wave decreased more severely, resulting in nearly complete abolishment of the b-wave as early as 1 day after $NaIO_3$ administration in both groups. At 4 days, the b-wave amplitudes began to be recovered, subsequently reaching the levels of the baseline at 7 days. Afterwards, restoration of both the a- and b-wave amplitudes was maintained until the end of the study at day 28.

3.2.2.2. Intermediate-dose $NaIO_3$ group (0.4mg)

In the 0.4-mg group, the a-wave amplitude was severely reduced relative to that of the baseline as early as 1 day after $NaIO_3$ injection, which condition was maintained without any restoration throughout the follow-up period. The b-wave amplitude was nearly completely abolished as early as 1 day, followed by merely detectable restoration after 4 days. However, the amplitudes of the b-wave remained at merely detectable levels throughout the study until day 28. Early loss of outer retinal laminations followed by subsequent destruction of inner retina in OCT and histologic findings would appear to correlate with persistent reduced amplitudes of both a- and b-waves.

3.2.2.3. High-dose $NaIO_3$ group (0.8mg)

In the 0.8-mg group, the a- and b-waves were completely undetectable throughout the entire follow-up periods after $NaIO_3$ injection.
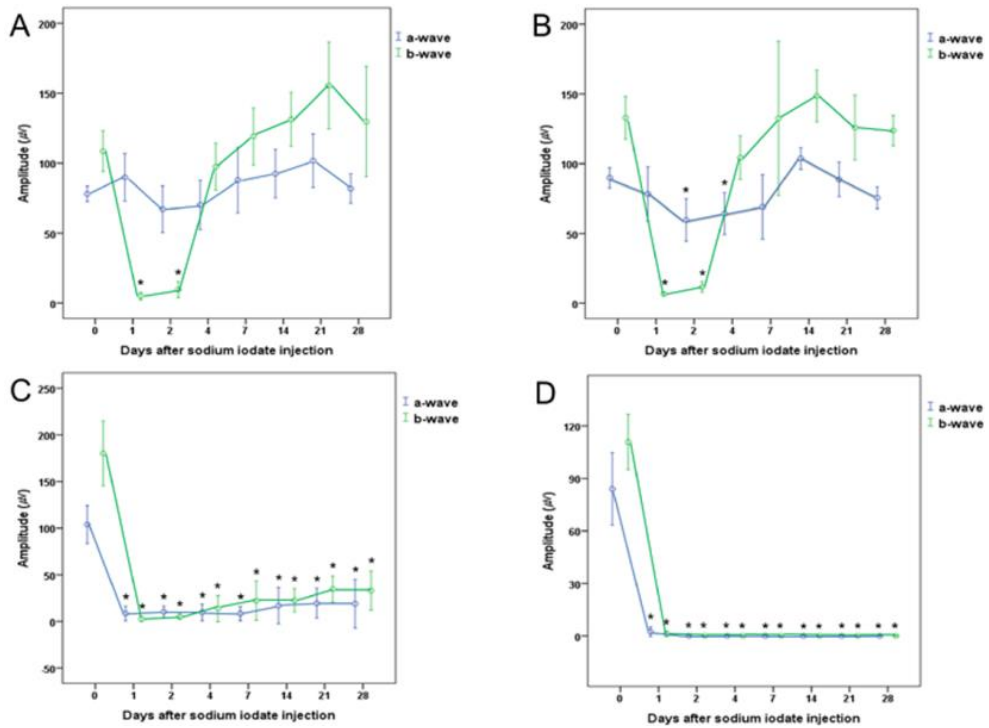
Figure 3-10. The serial changes of a- and b-wave amplitudes after intravitreal sodium iodate ($NaIO_3$) administration in rabbits. (A) 0.1-mg $NaIO_3$ group. (B) 0.2-mg $NaIO_3$ group. (C) 0.4-mg $NaIO_3$ group. (D) 0.8-mg $NaIO_3$ group. Values are expressed as means ± 2 standard errors. Asterisks mean $P < 0.05$ compared to baseline.

Chapter 4. Discussion

4.1. Surgical techniques to optimize the long-term outcomes of LCP-based retinal prosthesis

4.1.1. Pilot study

Our results showed that the surgical steps were successfully conducted without any intraoperative complications for the implantation of initial-version of LCP-based prosthetic device. During the follow-up periods up to 10 months, no clinically significant reactions of eyeball or head were detected under surgical microscope such as inflammation, infection, wound dehiscence, retinal detachment or intraocular hemorrhage. In addition, the OCT and x-ray images confirmed the proper position of electrode array in the suprachoroidal space and system package on the skull without any displacement of devices until the end of the study. Based on the experience of this pilot study, I established the basic surgical steps for long-term implantation of modified version of LCP-based prosthetic device.

4.1.2. Totally implantable LCP-based retinal prosthesis

The surgical techniques for implantation of the LCP-based retinal prosthesis were relatively safe and reproducible for the modified version of device. However, I experienced two cases of complications resulting from inappropriate advancement of the electrode array into the suprachoroidal space. In one case, I selected an

improper position of scleral incision, which was located too far posteriorly, resulting in failure to refine the electrode array insertion adequately and, thus, optic nerve damage. In another case, retinal tear developed as a result of the application of excessive force to push the electrode array into the suprachoroidal space. The monolithic fabrication process of LCP-based prosthesis includes the thermal bonding of LCP layers using a heating press.[39] A few LCP-based electrode array became slightly inflexible after thermal bonding process. Such an unexpected fabrication result might contribute to the development of retinal tear in case 10. Correct positioning of each component of the retinal prosthesis is critical to its successful implantation. A scleral incision approximately 3-5 mm from the limbus was suitable for sufficient modification of the directionality of the electrode array. The proper orientation of the electrode array for arrival at the predetermined site should be planned preoperatively based on dimensional information on both the specific eyeball and the device. If the implantation surgery is performed on 8-week-old rabbits, the following conditions would be suitable for electrode array to arrive properly under the visual streak: an LCP-based retinal prosthesis of 20 - 22 mm length and 65 - 70° angle between the electrode array and the transition part; a scleral incision 3 - 4 mm from the limbus and medial margin of the superior retractor bulbi muscle in the superonasal quadrant; complete insertion of the electrode array at the scleral incision to meet the transition part. Additionally, gentle manipulation with vigilant attention is needed to accomplish safe implantation of the retinal prosthesis without damage to the retina or device.

The implanted LCP-based retinal prosthesis was well tolerated for 3 months postoperatively. However, subsequently, a critical complication related to the extraocular components of the device began to manifest: conjunctival erosion or dehiscence over the package or transition part. Conjunctival erosion or dehiscence, followed by device exposure, has been a persistent complication related to extraocularly implanted devices such as glaucoma drainage devices and retinal prostheses. As previously reported, our LCP-based retinal prosthesis is geometrically comparable to the Ahmed Glaucoma Valve (Model FP7, New World Medical Inc., Rancho Cucamonga, CA, USA) (dimensions: 16 mm x 13 mm x 2.1 mm).[39] Reported incidences of conjunctival erosion over glaucoma drainage device have been as high as 30%.[42] Rates of device exposure have been reduced by the introduction of patch grafts such as those based on the human sclera[43] and human pericardium.[44] Despite such technical improvements, however, exposure of device remains one of the most common complications after implantation surgery of glaucoma drainage device. Similarly to the case of glaucoma drainage device, conjunctival erosion or dehiscence over a retinal prosthetic device has been the most prevalent adverse event in most clinical trials, with reported rates of 23.3% (7 of 30 subjects) for Argus II (Second Sight, Sylmar, CA, USA)[10] and 55.6% (5 of 9 subjects) among a Tübingen patient group for Retinal Implant Alpha IMS (Retinal Implant AG, Reutlingen, Germany).[18]

Several mechanisms for conjunctival erosion or dehiscence can be postulated, including mechanical friction of the eyelid and the tension of device to the

conjunctiva, particularly in cases of exposure of the transition part. In the present study, I attempted to anchor the transition part completely to the sclera with additional fixation sutures, but bulging of the transition part lead to excessive tension to the overlying conjunctiva. Such bulging can be ameliorated by covering the transition part by the superior retractor bulbi muscle or patch graft using donor sclera or by utilization of a modified design for complete attachment to the sclera. In one case (case 5), the transition part of device was passed under the retractor bulbi muscle, resulting in excellent long-term safety of device without any conjunctival erosion or dehiscence. However, this procedure might lead to inadvertent damage to the device. Thus, in the future, I will try to detach the retractor bulbi muscle before anchoring the device onto the sclera followed by reattachment of muscle to minimize the damage to the device. However, in the present study, the mechanism of conjunctival dehiscence over the package was presumed to be different. The rabbit, compared with humans, has compressed dimensions in its antero-posterior axis, with a shorter axial length of 16-19 mm and a larger and steeper cornea,[45] whereas the dummy devices used in our study had been manufactured to fit conformably to the human eyeball. The fixation sutures along the margin of the package became detached. Then, the displacement of package began to progress, leading to the development of conjunctival dehiscence. In summary, the dummy device was pushed forward, followed by its detachment due to the configuration mismatch between it and the rabbit's eyeball. This problem is resolvable by revision of the device configuration for conformal attachment to the rabbit eyeball.

Many technical challenges remain for the improved long-term safety of implantation surgery and the biostability of prosthetic devices. Device miniaturization is one of the key priorities. The initial version of the epiretinal prosthesis, Argus I, is interfaced with a 16-platinum-electrode array embedded in a silicone rubber platform.[46] Its intraocular components include an electrode array less than 1-mm thick and, extending from it, a 600 μm diameter cable that might be too bulky for intraocular implantation.[47] Meanwhile, the initial subretinal prosthesis version, Alpha IMS, consists of a silicon-based microphotodiode array chip embedded between polyimide layers of approximately 70 μm thickness. The current version of the epiretinal implant, Argus II, with its flexible polyimide-based microelectrode array,[19] is thinner than the previous version. Presently, a parylene-based electrode array for better hermetic sealing is under investigation.[48] Traditionally, hermetic enclosures packaging electronics are formed of titanium (Argus II) or ceramic (Argus I and Alpha IMS) and joined to a feedthrough to deliver electrical signals to the electrode array.[49] Feedthrough technologies, however, with their increasing number of stimulation channels, hinder the device miniaturization that is essential to the development of high-density electrode arrays. Our group offers outstanding prosthetic-device miniaturization relative to the leading groups. Our group successfully manufactured a monolithically encapsulated LCP-based retinal prosthesis that does not require any feedthrough and that, accordingly, allows for further miniaturization comparable to the Ahmed Glaucoma Valve. Additionally, our group realized a further reduction of electrode-

array thickness, to 30 μm, by means of an advanced fabrication process such as laser-machining.[40] Furthermore, the long-term reliability of our device, achieved through adequate hermetic sealing, has already been established in a previous report.[6]

4.2. Anatomic correlations with retinal changes seen on OCT in NaIO$_3$-induced retinal degeneration

In this study, I investigated the histologic correlations with several abnormal OCT features shown in experimental retinal degeneration. The most interesting findings were the histologic correlations with outer retinal changes on OCT images, such as the disrupted EZ or ELM in the early phases of 0.2- and 0.4-mg NaIO$_3$-induced retinal degeneration. In those cases, the histologic analysis could not clearly elucidate the pathologic features of the OCT images. In the 0.2-mg group, the ELM became hardly detectable, with a slightly obscure EZ on the 4th day following injection of NaIO$_3$, without notable changes to the retina in histologic sections, but recovered gradually, leading to nearly complete restoration of intensity and integrity of both the ELM and EZ on OCT. Meanwhile, in the 0.4-mg group, the outer photoreceptor layer with alternating hypo- and hyper-reflective bands under normal conditions was replaced with a diffuse hyper-reflective zone with indistinguishable EZ and ELM as early as 1 day after NaIO$_3$ injection. However, the histological analysis represented only slightly disorganized arrangement of photoreceptor IS and OS, with relatively preserved overall laminations of

photoreceptor cell nuclei, IS and OS until day 2. Taking all of the results together, I speculated that the OCT can reflect early ultrastructural changes of photoreceptors manifesting as disrupted EZ and ELM prior to overt morphological changes in histologic sections. The subtle changes of the EZ on OCT images in the 0.2-mg group might reflect reversible and minimal changes of photoreceptors that are not sufficient to induce irreversible dysfunction of photoreceptors that are supported by the complete restoration of a-waves in the dark-adapted ERG. In the 0.4-mg group by contrast, the evident changes of the outer retinal layers on OCT images might suggest critical and irreversible impairment of photoreceptors, resulting in their complete dysfunction, as confirmed by the extreme reduction of a-wave amplitudes and subsequent photoreceptor cell death.

Traditionally, the oxidizing agent $NaIO_3$ has been known to target RPE cells primarily, leading to secondary photoreceptor apoptosis.[22,50] In RPE cells, impairment of cytoplasmic organelles such as mitochondrial dysfunction has been reported to precede cell death induced by $NaIO_3$,[51,52] which finding is similar to that of previous report on mitochondrial swelling of RPE cells on electron microscopy.[27] Several recent studies however have reported acute direct effects of $NaIO_3$ on the inner retina, such as hydropic changes of photoreceptors, prior to overt RPE damage.[23,24,53] In addition, a few studies utilizing transgenic animal models for retinal degeneration might provide clues to the pathophysiology of abnormal OCT features,[54,55] though the mechanism of retinal degeneration in transgenic animals differs from that of $NaIO_3$-induced degeneration. Muraoka et

al.[55] reported, similarly to the results of this dissertation, hyper-reflective change in the outer photoreceptor layer with indistinguishable EZ, but with almost-intact photoreceptor IS and OS on histological analysis in the early phase of experimental retinal degeneration of transgenic rabbits. Ultrastructural damage to photoreceptors has been cited as the cause of a highly reflective outer photoreceptor layer such as by accumulation of numerous extracellular vesicles cleaved from the membrane of the IS regardless of the relatively well-packed disc of the OS.[54, 55] Taken together, I speculated that the toxicity of $NaIO_3$ might induce acute mitochondrial dysfunction in the photoreceptor IS ellipsoid, which is the origin of a highly reflective EZ on OCT imaging,[56] prior to overt RPE degeneration. Increased intracellular production of reactive oxygen species (ROS) by $NAIO_3$ as predominantly localized to the mitochondria in αB crystalline siRNA-transfected RPE cells, has been reported as well.[57] This might also be true for photoreceptors, and if so, it might explain the altered reflectivity of the EZ in OCT images. In addition, a damaged photoreceptor IS might contribute to rapid disruption of outer retinal bands and subsequent photoreceptor degeneration as seen on OCT imaging.

In the present study, I found increased reflectivity of the ONL, which was relatively hypo-reflective under normal physiologic conditions, in the 0.4-mg NaIO3-treated rabbits. However, at this time point, the histologic section showed relatively well-preserved photoreceptor cell nuclei in the ONL despite moderate swelling of the retina. Several studies have demonstrated transient ONL hyper-reflectivity followed by gradual reduction of retinal thickness in OCT, as consistent

with our results.[53,58] Machalińska et al.[58] suggested that a hyper-reflective ONL could be attributed to apoptotic cell death of photoreceptors with cellular disorganization, as detected by TUNEL assay. Thus, I speculated that the OCT could also detect the early phase of photoreceptor degeneration as increased reflectivity of the ONL prior to the appearance of distinct ONL changes in H&E-stained sections.

The data of this dissertation detected attenuated retinal function characterized by nearly complete loss of the b-wave as early as 1 day after $NAIO_3$ injection, regardless of morphologic changes on OCT images or in histologic sections. Even the 0.1-mg $NAIO_3$-treated rabbits showed nearly complete abolishment of b-waves, in contrast to the relatively well-preserved a-waves in the early phase of the experiments, though there were no obvious morphologic changes in either the OCT or histologic analysis. Previous reports have demonstrated early ERG changes characterized by reduction of the b/a amplitude ratio even prior to distinct morphologic changes to the retina.[23, 25, 59] Several explanations for these results have been proposed, including defective synaptic transmission to bipolar cells,[23] primary damage to rods with relatively maintained cone function,[25] or relative preservation of the third-order neuronal response despite functional damage to photoreceptors.[59] However, the pathophysiology of these results remains uncertain. Further experiments entailing *ex vivo* patch clamp or multichannel analysis with neurotransmission blocker would be needed to support the hypotheses.

This study has several limitations. First of all, I did not provide evidence of

ultrastructural changes of photoreceptors directly related to abnormal OCT findings, which changes could not be explained by the histologic analysis in our experiments. Further experiments are required to elucidate the mechanism of discrepancy between OCT and histologic results in NAIO$_3$-induced retinal degeneration, though I were able to inferred some of that from previous reports of retinal degeneration studies with transgenic rabbits.[54,55] In addition, the number of subjects was small, and the data, as obtained from only albino rabbits, might not be sufficient for extrapolation to different species including humans.

Chapter 5. Conclusion

In the present preclinical study, I investigated safe and reproducible surgical techniques for implantation of our LCP-based retinal prosthesis into the suprachoroidal space. Issues related to surgical technique or device configuration were identified, including intraocular trauma related to electrode array insertion and conjunctival erosion/dehiscence over the extraocular components of the device, respectively. However, I expect that the technical solutions suggested herein with superiority of our miniaturized device, will improve the long-term safety of its implantation. Finally, these experiments would provide a stepping stone to achieve the safe and reproducible surgical techniques for human in the future.

Next, I determined that *in vivo* imaging by OCT can facilitate detection of early ultrastructural changes of photoreceptors, manifesting as disrupted EZ and ELM, prior to overt morphological changes in histologic sections. Additionally, I found that the degree of morphologic change of the outer retina on OCT images might provide clues to the severity of retinal impairment and whether or not recovery is possible. Furthermore, in the future, these results on experimental retinal degeneration could be applied clinically for evaluation of pathological changes of the retina in patients with degenerative conditions such as retinitis pigmentosa.

References

1.	Santos A, Humayun MS, de Juan E, Jr., et al. Preservation of the inner retina in retinitis pigmentosa. A morphometric analysis. Arch Ophthalmol 1997;115:511-5.

2.	Kim SY, Sadda S, Humayun MS, de Juan E, Jr., Melia BM, Green WR. Morphometric analysis of the macula in eyes with geographic atrophy due to age-related macular degeneration. Retina 2002;22:464-70.

3.	Maynard EM. Visual prostheses. Annu Rev Biomed Eng 2001;3:145-68.

4.	Chen MJ, Pham AVH, Evers NA, et al. Design and development of a package using LCP for RF/Microwave MEMS switches. IEEE T Microw Theory 2006;54:4009-15.

5.	Jeong J, Lee SW, Min KS, Shin S, Jun SB, Kim SJ. Liquid cyrstal polymer (LCP), an attractive substrate for retinal implant. Sensors and Materials 2012;24:189-203.

6.	Jeong J, Hyun Bae S, Seo JM, Chung H, June Kim S. Long-term evaluation of a liquid crystal polymer (LCP)-based retinal prosthesis. J Neural Eng 2016;13:025004.

7.	Jeong J, Lee SW, Min K, Eom K, Bae SH, Kim SJ. Eye-surface conformable telemetric structure for polymer-based retinal prosthesis. Conf Proc IEEE Eng Med Biol Soc 2011;2011:1097-100.

8.	Jeong J, Lee SW, Min KS, Kim SJ. A novel multilayered planar coil based on biocompatible liquid crystal polymer for chronic implantation. Sensors and Actuators A: Physical 2013;197:38-46.

9.	Humayun MS, de Juan E, Jr., Dagnelie G. The Bionic Eye: A Quarter Century of Retinal Prosthesis Research and Development. Ophthalmology 2016;123:S89-S97.

10.	da Cruz L, Dorn JD, Humayun MS, et al. Five-Year Safety and Performance Results from the Argus II Retinal Prosthesis System Clinical Trial. Ophthalmology 2016;123:2248-54.

11.	Edwards TL, Cottriall CL, Xue K, et al. Assessment of the Electronic Retinal Implant Alpha AMS in Restoring Vision to Blind Patients with End-Stage Retinitis Pigmentosa. Ophthalmology 2018;125:432-43.

12.	Zrenner E. Fighting blindness with microelectronics. Sci Transl Med 2013;5:210ps16.

13.	Stingl K, Schippert R, Bartz-Schmidt KU, et al. Interim Results of a Multicenter Trial with the New Electronic Subretinal Implant Alpha AMS in 15 Patients Blind from Inherited Retinal Degenerations. Front Neurosci 2017;11:445.

14.	Ayton LN, Blamey PJ, Guymer RH, et al. First-in-human trial of a novel suprachoroidal retinal prosthesis. PLoS One 2014;9:e115239.

15.	Fujikado T, Kamei M, Sakaguchi H, et al. One-Year Outcome of 49-Channel Suprachoroidal-Transretinal Stimulation Prosthesis in Patients With Advanced Retinitis Pigmentosa. Invest Ophthalmol Vis Sci 2016;57:6147-57.

16.	Roessler G, Laube T, Brockmann C, et al. Angiographic findings

following tack fixation of a wireless epiretinal retina implant device in blind RP patients. Graefes Arch Clin Exp Ophthalmol 2011;249:1281-6.

17.	Gekeler F, Kobuch K, Schwahn HN, Stett A, Shinoda K, Zrenner E. Subretinal electrical stimulation of the rabbit retina with acutely implanted electrode arrays. Graefes Arch Clin Exp Ophthalmol 2004;242:587-96.

18.	Kitiratschky VB, Stingl K, Wilhelm B, et al. Safety evaluation of "retina implant alpha IMS"--a prospective clinical trial. Graefes Arch Clin Exp Ophthalmol 2015;253:381-7.

19.	Luo YH, da Cruz L. The Argus((R)) II Retinal Prosthesis System. Prog Retin Eye Res 2016;50:89-107.

20.	Roessler G, Laube T, Brockmann C, et al. Implantation and explantation of a wireless epiretinal retina implant device: observations during the EPIRET3 prospective clinical trial. Invest Ophthalmol Vis Sci 2009;50:3003-8.

21.	Rizzo JF, 3rd. Update on retinal prosthetic research: the Boston Retinal Implant Project. J Neuroophthalmol 2011;31:160-8.

22.	Kiuchi K, Yoshizawa K, Shikata N, Moriguchi K, Tsubura A. Morphologic characteristics of retinal degeneration induced by sodium iodate in mice. Curr Eye Res 2002;25:373-9.

23.	Wang J, Iacovelli J, Spencer C, Saint-Geniez M. Direct effect of sodium iodate on neurosensory retina. Invest Ophthalmol Vis Sci 2014;55:1941-53.

24.	Tao Z, Dai J, He J, Li C, Li Y, Yin ZQ. The influence of NaIO(3)-induced retinal degeneration on intra-retinal layer and the changes of expression profile/morphology of DA-ACs and mRGCS. Mol Neurobiol 2013;47:241-60.

25.	Machalinska A, Lubinski W, Klos P, et al. Sodium iodate selectively injuries the posterior pole of the retina in a dose-dependent manner: morphological and electrophysiological study. Neurochem Res 2010;35:1819-27.

26.	Chowers G, Cohen M, Marks-Ohana D, et al. Course of Sodium Iodate-Induced Retinal Degeneration in Albino and Pigmented Mice. Invest Ophthalmol Vis Sci 2017;58:2239-49.

27.	Cho BJ, Seo JM, Yu HG, Chung H. Monocular retinal degeneration induced by intravitreal injection of sodium iodate in rabbit eyes. Jpn J Ophthalmol 2016;60:226-37.

28.	Staurenghi G, Sadda S, Chakravarthy U, Spaide RF, International Nomenclature for Optical Coherence Tomography P. Proposed lexicon for anatomic landmarks in normal posterior segment spectral-domain optical coherence tomography: the IN*OCT consensus. Ophthalmology 2014;121:1572-8.

29.	Oishi A, Tsujikawa A, Yamashiro K, et al. One-year result of aflibercept treatment on age-related macular degeneration and predictive factors for visual outcome. Am J Ophthalmol 2015;159:853-60 e1.

30.	Shen Y, Liu K, Xu X. Correlation Between Visual Function and Photoreceptor Integrity in Diabetic Macular Edema: Spectral-Domain Optical Coherence Tomography. Curr Eye Res 2016;41:391-9.

31.	Brown NH, Koreishi AF, McCall M, Izatt JA, Rickman CB, Toth CA. Developing SDOCT to assess donor human eyes prior to tissue sectioning for research. Graefes Arch Clin Exp Ophthalmol 2009;247:1069-80.

32.	Bagheri N, Bell BA, Bonilha VL, Hollyfield JG. Imaging human postmortem eyes with SLO and OCT. Adv Exp Med Biol 2012;723:479-88.

33.	Toth CA, Narayan DG, Boppart SA, et al. A comparison of retinal morphology viewed by optical coherence tomography and by light microscopy. Arch Ophthalmol 1997;115:1425-8.

34.	Huang Y, Cideciyan AV, Papastergiou GI, et al. Relation of optical coherence tomography to microanatomy in normal and rd chickens. Invest Ophthalmol Vis Sci 1998;39:2405-16.

35.	Lee SW, Seo JM, Ha S, Kim ET, Chung H, Kim SJ. Development of microelectrode arrays for artificial retinal implants using liquid crystal polymers. Invest Ophthalmol Vis Sci 2009;50:5859-66.

36.	Lee SW. Development of long-term implantable neuroprosthetic devices using liquid crystal polymer (LCP). Ph D Dissertation, Seoul National University, Seoul, Korea 2010.

37.	Gekeler F, Szurman P, Grisanti S, et al. Compound subretinal prostheses with extra-ocular parts designed for human trials: successful long-term implantation in pigs. Graefes Arch Clin Exp Ophthalmol 2007;245:230-41.

38.	Morimoto T, Kamei M, Nishida K, et al. Chronic implantation of newly developed suprachoroidal-transretinal stimulation prosthesis in dogs. Invest Ophthalmol Vis Sci 2011;52:6785-92.

39.	Jeong J, Bae SH, Min KS, Seo JM, Chung H, Kim SJ. A miniaturized, eye-conformable, and long-term reliable retinal prosthesis using monolithic fabrication of liquid crystal polymer (LCP). IEEE Trans Biomed Eng 2015;62:982-9.

40.	Jeong J, Shin S, Lee G, Gwon T, Park J, Kim S. Advancements in fabrication process of microelectrode array for a retinal prosthesis using Liquid Crystal Polymer (LCP). Conf Proc IEEE Eng Med Biol Soc 2013;2013:5295-8.

41.	McCulloch DL, Marmor MF, Brigell MG, et al. ISCEV Standard for full-field clinical electroretinography (2015 update). Doc Ophthalmol 2015;130:1-12.

42.	Christakis PG, Kalenak JW, Zurakowski D, et al. The Ahmed Versus Baerveldt study: one-year treatment outcomes. Ophthalmology 2011;118:2180-9.

43.	Freedman J. Scleral patch grafts with Molteno setons. Ophthalmic Surg 1987;18:532-4.

44.	Raviv T, Greenfield DS, Liebmann JM, Sidoti PA, Ishikawa H, Ritch R. Pericardial patch grafts in glaucoma implant surgery. J Glaucoma 1998;7:27-32.

45.	Gwon A. The rabbit in cataract/IOL surgery. Panagiotis AT. Animal model in eye research. New York: Elsevier; 2008:184-204.

46.	de Balthasar C, Patel S, Roy A, et al. Factors affecting perceptual thresholds in epiretinal prostheses. Invest Ophthalmol Vis Sci 2008;49:2303-14.

47.	Majji AB, Humayun MS, Weiland JD, Suzuki S, D'Anna SA, de Juan E, Jr. Long-term histological and electrophysiological results of an inactive epiretinal electrode array implantation in dogs. Invest Ophthalmol Vis Sci 1999;40:2073-81.

48.	Rodger DC, Fong AJ, Li W, et al. Flexible parylene-based multielectrode array technology for high-density neural stimulation and recording. Sensors and Actuators B: Chemical 2008;132:449-60.

49.   Yue L, Weiland JD, Roska B, Humayun MS. Retinal stimulation strategies to restore vision: Fundamentals and systems. Prog Retin Eye Res 2016;53:21-47.

50.   Yang Y, Ng TK, Ye C, et al. Assessing sodium iodate-induced outer retinal changes in rats using confocal scanning laser ophthalmoscopy and optical coherence tomography. Invest Ophthalmol Vis Sci 2014;55:1696-705.

51.   Juel HB, Faber C, Svendsen SG, Vallejo AN, Nissen MH. Inflammatory cytokines protect retinal pigment epithelial cells from oxidative stress-induced death. PLoS One 2013;8:e64619.

52.   Nilsson SE, Knave B, Persson HE. Changes in ultrastructure and function of the sheep pigment epithelium and retina induced by sodium iodate. I. The ultrastructure of the normal pigment epithelium of the sheep. Acta Ophthalmol (Copenh) 1977;55:994-1006.

53.   Hariri S, Tam MC, Lee D, Hileeto D, Moayed AA, Bizheva K. Noninvasive imaging of the early effect of sodium iodate toxicity in a rat model of outer retina degeneration with spectral domain optical coherence tomography. J Biomed Opt 2013;18:26017.

54.   Kondo M, Sakai T, Komeima K, et al. Generation of a transgenic rabbit model of retinal degeneration. Invest Ophthalmol Vis Sci 2009;50:1371-7.

55.   Muraoka Y, Ikeda HO, Nakano N, et al. Real-time imaging of rabbit retina with retinal degeneration by using spectral-domain optical coherence tomography. PLoS One 2012;7:e36135.

56.   Spaide RF, Curcio CA. Anatomical correlates to the bands seen in the outer retina by optical coherence tomography: literature review and model. Retina 2011;31:1609-19.

57.   Zhou P, Kannan R, Spee C, Sreekumar PG, Dou G, Hinton DR. Protection of retina by alphaB crystallin in sodium iodate induced retinal degeneration. PLoS One 2014;9:e98275.

58.   Machalinska A, Lejkowska R, Duchnik M, et al. Dose-dependent retinal changes following sodium iodate administration: application of spectral-domain optical coherence tomography for monitoring of retinal injury and endogenous regeneration. Curr Eye Res 2014;39:1033-41.

59.   Tanaka M, Machida S, Ohtaka K, Tazawa Y, Nitta J. Third-order neuronal responses contribute to shaping the negative electroretinogram in sodium iodate-treated rats. Curr Eye Res 2005;30:443-53

요약(국문초록)

본 연구진은 액정폴리머 기반의 일체형 인공망막장치를 개발하였는데, 이는 세라믹 또는 금속으로 만들어진 기존의 신경보철장치에 비해 얇고 가볍다는 장점이 있다. 그러나 인공망막장치 체내 삽입술은 고난위도의 수술기법을 요구하므로, 장기간 체내 안전성을 확보하기 위한 수술기법을 확립하기 위해서는 아직 많은 노력이 필요하다. 본 논문에서는 동물실험을 통해 액정폴리머 기반의 인공망막장치의 장기간 안전성을 최적화하기 위한 수술기법을 개발하고자 하였다. 예비연구에서 프로토타입 인공망막장치를 2마리의 토끼에 삽입하였다. 전극은 맥락막상강으로 삽입하고 시스템 패키지는 두개골 위에 장착하였다. 전극과 패키지 사이의 연결부는 안와 주변의 조직을 박리한 뒤 측두근 아래로 통과시켰다. 삽입술은 합병증 없이 성공적으로 시행되었다. 수술 후 시행한 안저검사, 빛간섭단층촬영과 X-선 촬영에서도 안내출혈, 망막박리, 절개부 벌어짐, 장치 이탈 등의 합병증은 관찰되지 않았다. 다음으로 액정폴리머 기반의 인공망막장치의 형태를 개선하여 안구에 완전히 이식할 수 있도록 수정하고, 11마리의 토끼에서 삽입술을 시행하였다. 전극은 맥락막상강으로 삽입하고, 패키지는 공막에 고정하였으며, 전극과 패키지 사이의 이행부는 공막에 고정하였다. 삽입술은 9마리(81.8%)에서 합병증 없이 성공적

으로 이루어졌다. 그러나 2마리(18.2%)에서는 전극삽입 중 시신경 손상 및 망막 열공의 합병증이 발생하였다. 술 후 적어도 3개월동안은 10마리(90.9%)에서 인공망막장치가 체내에서 안정적으로 유지되었다. 그러나 3개월 후 9마리(81.8%)에서 패키지 또는 이행부를 덮은 결막의 미란 또는 벌어짐이 확인되었다. 그러나 이와 관계없이 맥락막상강에 삽입된 전극은 술 후에도 부작용 없이 안정적으로 유지되었다. 본 연구를 통해 수술기법 또는 장치의 형태와 관련된 몇몇 문제를 확인하였고, 추후 기술적인 개선책으로 인공망막장치 체내 삽입술의 장기간 안전성을 향상시킬 수 있을 것으로 기대한다. 또한 궁극적으로 사람에서 안전하게 인공망막장치를 삽입할 수 있는 수술기법 개발의 디딤돌이 될 것으로 기대한다.

사람과 동물모델을 기반으로 많은 연구들이 이루어져왔지만, 망막변성 질환의 병태생리는 아직 명확히 밝혀지지 않았다. 생체내 망막의 구조적 변화에 대한 연구는 망막변성질환의 발병 및 진행을 이해하는데 중요하다. 근래에 빛간섭단층촬영은 망막 구조에 대한 생체연구에서 가장 유용한 검사법이지만, 아직 망막변성질환에서 비정상적인 빛간섭단층촬영 소견에 부합하는 해부학적 소견에 대해서는 명확히 알려지지 않았다. 본 논문에서는 유리체강내 요오드산나트륨을 주입한 토끼 망막변성모델에서 망막전위도 검사결과로 뒷받침되는 빛간섭단층촬영에서의 병적 변화에 부합하는 해부학적 소견을 분석하고자 하였다. 20마리의 토끼를 5마리씩

4군으로 나누어, 각 토끼의 단안에 요오드산나트륨을 군별로 0.1, 0.2, 0.4, 또는 0.8mg을 유리체강내 주입하였다. 투여 전 및 투여 후 28일 동안 각 토끼는 안저검사, 빛간섭단층촬영, 망막전위도 및 조직학적 검사를 시행하였다. 요오드산나트륨 0.2mg 군에서는 빛간섭단층촬영상 외경계막 소실 및 경도의 불분명한 타원체구역의 소견이 일시적으로 관찰되었으나, 조직학적 검사에서는 명확한 변화는 확인되지 않았다. 망막전위도 검사상 초기의 일시적인 a-파와 b-파의 감소는 투여 후 28일경에는 완전히 회복되었다. 0.4mg 군에서는 투여 후 1일째부터 빛간섭단층촬영상 외경계막 및 타원체구역이 소실되었지만, 초기 조직학적 검사에서는 빛수용세포의 핵, 내절 및 외절의 층판 구조는 비교적 유지되고 경도의 외절 및 내절의 구조적 손상만 관찰되었다. 이후에는 빛간섭단층촬영 및 조직학적 검사상 외망막층의 손상은 진행되어, 투여 후 28일경에는 빛수용세포는 완전히 소실되었다. 망막전위도 검사에서는 경과관찰 기간 동안 심한 a-파 및 b-파의 진폭의 감소가 지속되었다. 결론적으로 본 논문에서 빛간섭단층촬영은 조직학적 검사상 명확한 해부학적 변화가 나타나기 이전에 빛수용세포의 초미세구조의 변화를 초기에 확인할 수 있었다. 또한 빛간섭단층촬영상 외경계막 및 타원체구역의 손상 정도로 빛수용세포가 손상된 정도를 예측할 수 있었다.

주요어 : 인공망막장치, 액정폴리머, 삽입술, 요오드산나트륨, 망막변성

학번 : 2012-30271